Microglia induce motor neuron death via the classical NF-κB pathway in amyotrophic lateral sclerosis

Ashley E. Frakes[1,2], Laura Ferraiuolo[1], Amanda M. Haidet-Phillips[1], Leah Schmelzer [1], Lyndsey Braun [1], Carlos J. Miranda[1], Katherine J. Ladner[5], Adam Bevan[1,2], Kevin D. Foust[4], Jonathan P. Godbout[4], Phillip G. Popovich[4], Denis C. Guttridge[5], Brian K. Kaspar [1,2,4,†]

[1] Center for Gene Therapy, The Research Institute at Nationwide Children's Hospital, Columbus, OH

[2] Biomedical Sciences Graduate Program, College of Medicine, The Ohio State University, Columbus, OH

[4] Department of Neuroscience, The Ohio State University, Columbus, OH 43205

[5] Department of Molecular Virology, Immunology and Medical Genetics, The Ohio State University, Columbus, OH 43210

For Submission as an article to *Neuron*

† To whom correspondence should be addressed:

Brian K. Kaspar, Ph.D.

700 Children's Drive WA 3022

Columbus, OH 43205

(ph) 614.722.5085

(fax)614.355.5247

Email: Brian.Kaspar@NationwideChildrens.org

SUMMARY

Neuroinflammation is one of the most striking hallmarks of amyotrophic lateral sclerosis (ALS). Nuclear Factor-kappa B (NF-κB), a master regulator of inflammation, is upregulated in spinal cords of ALS patients and SOD1-G93A mice. In this study, we show that selective NF-κB inhibition in ALS astrocytes is not sufficient to rescue motor neuron (MN) death. However, the localization of NF-κB activity and subsequent deletion of NF-κB signaling in microglia led to rescued MNs from microglial-mediated death *in vitro* and extended survival in ALS mice by impairing pro-inflammatory microglial activation. Conversely, constitutive activation of NF-κB selectively in WT microglia induced gliosis and MN death *in vitro* and *in vivo.* Taken together, these data provide a mechanism by which microglia induce MN death in ALS, and suggest a novel therapeutic target that can be modulated to slow the progression of ALS and possibly other neurodegenerative diseases by which microglial activation plays a role.

INTRODUCTION

Amyotrophic lateral sclerosis (ALS) is a devastating, fast-progressing neurodegenerative disease characterized by motor neuron (MN) death in the brainstem, spinal cord, and motor cortex. Typically within 2-5 years of clinical onset, patients succumb to the disease due to severe muscle atrophy, paralysis, and ultimately denervation of respiratory muscles. Most ALS cases are classified as sporadic, defined as having no family history of the disease. The remaining 5-10% of cases are classified as familial and are typically inherited in an autosomal dominant fashion. Despite genetic differences, these two forms of ALS are clinically indistinguishable. Approximately 20% of familial cases are associated with mutations in the gene superoxide dismutase 1 (SOD1) (Rosen et al., 1993). Transgenic rodents carrying mutant forms of SOD1 develop a similar, progressive MN disease akin to patients and are used as the gold standard in ALS research. Elegant studies using these animals have shown that non-neuronal cells play a crucial role in ALS, contributing to MN death via non-cell autonomous mechanisms (Clement et al., 2003). Similarly, *in vitro* studies have shown that murine astrocytes and microglia expressing mutant SOD1 and human astrocytes from sporadic and familial ALS patients can induce MN death (Di Giorgio et al., 2008; 2007; Haidet-Phillips et al., 2011; Marchetto et al., 2008; Nagai et al., 2007; Xiao et al., 2007). Evidence that individual cell types mediate different aspects of disease emerged from the generation of mice expressing a conditional deletion of the mutant SOD1 gene. Removal of mutant SOD1 specifically in MNs extended survival by delaying disease onset and early disease progression, while excising flox'ed mutant SOD1 in either microglia/macrophages or astrocytes extended survival by slowing disease progression, but not onset (Boillee et al., 2006; Yamanaka et al., 2008). Similarly, replacing the myeloid lineage of mutant SOD1 mice with WT microglia/macrophages slowed disease progression (Beers et al., 2006). This suggests ALS is a deadly convergence of damage developed in multiple cellular compartments that ultimately leads to neuromuscular failure. However, the precise mechanisms by which individual cell types such as astrocytes and microglia contribute to the disease remain unknown.

One of the most striking hallmarks of ALS shared by familial and sporadic patients as well as rodent models is neuroinflammation, characterized by extensive astrogliosis, microglial activation, and infiltration of peripheral immune cells at sites of neurodegeneration (Alexianu et al., 2001; Hall et al., 1998; Kawamata et al.,

1992; Mantovani et al., 2009; Turner et al., 2004). Mutant SOD1 astrocytes and microglia exhibit increased expression of many pro-inflammatory genes (Philips and Robberecht, 2011). However, genetic approaches to globally eliminate single inflammatory genes in ALS mouse models have largely failed to extend survival (Almer et al., 2006; Gowing et al., 2006; Nguyen et al., 2001; Son et al., 2001) and in some cases have even hastened disease progression (Lerman et al., 2012), highlighting the complexity of neuroinflammation in ALS. For these reasons a successful therapeutic approach is likely to derive from a better understanding of the intricate molecular mechanisms driving the inflammatory response and the identification of up-stream transcription factors that are dysregulated in each cellular compartment throughout the course of disease.

Classical NF-κB signaling involving the p65/p50 heterodimer is a major regulator of inflammation, driving gene expression of pro-inflammatory cytokines, chemokines, enzymes and adhesion molecules, many of which are upregulated in ALS. When inflammatory mediators bind their respective receptors, a signaling cascade is initiated that leads to phosphorylation and activation of IKKβ (a subunit of the inhibitor of IκB kinase, IKK, complex). Activated IKKβ phosphorylates the IκB inhibitory protein IκBα, targeting it for ubiquitination and proteasomal degradation, and subsequent release of NF-κB (p65/p50) to the nucleus where it binds to its cognate DNA sequences to induce gene expression (Ghosh and Karin, 2002). Additionally, phosphorylation at specific serine residues by IKKβ are required for transactivation function of the p65 subunit of NF-κB (Hayden and Ghosh, 2008). We previously reported NF-κB as the highest-ranked regulator of inflammation by Ingenuity Pathway analysis of inflammatory gene array data from astrocytes derived from human post mortem ALS patients (Haidet-Phillips et al., 2011). Other laboratories have confirmed by immunohistochemistry that NF-κB is activated in glia in familial and sporadic ALS patients (Swarup et al., 2011). Interestingly, loss of function mutations in the gene optineurin, which is known to negatively regulate TNF-α-induced NF-κB activation, have been found in ALS patients (Maruyama et al., 2011). However, it remains unknown whether NF-κB activation in ALS glia is involved in MN death.

Since the role of glial-derived inflammation in ALS remains ambiguous, we sought to determine whether inflammatory signaling regulated by NF-κB in astrocytes and microglia mediates MN death in ALS. In the current study we demonstrate that NF-κB is activated with disease progression in the SOD1-G93A mouse

model, specifically in glia. In agreement with recent publications, inhibition of NF-κB in astrocytes, using both transgenic and viral-mediated gene delivery approaches, did not increase motor function or survival in our SOD1-G93A mice (Crosio et al., 2011a). However, inhibition of NF-κB selectively in microglia, rescues MN survival *in vitro*, and *in vivo* extends survival in the ALS mice by delaying disease progression by 47%, one of the longest extensions reported in this severe model. NF-κB inhibition in microglia leads to marked reduction in prototypic inflammatory markers, suggesting that NF-κB regulates microglial conversion to a pro-inflammatory, neurotoxic state in ALS. Conversely, we show that constitutive activation of NF-κB selectively in myeloid cells in WT mice creates the pathological features of ALS in the spinal cord, i.e., gliosis and MN death. Together, these data indicate that NF-κB activation in microglia is a novel molecular mechanism underlying MN death in ALS. Moreover, the data identify a new therapeutic target to modulate microglial activation and slow the progression of ALS and other neurodegenerative diseases in which microglial activation plays a role.

RESULTS

NF-κB is activated with disease progression in the SOD1-G93A mouse model of ALS

In order to gain insight into NF-κB regulation in ALS, we performed electrophoretic mobility shift assay (EMSA) analysis on whole spinal cord nuclear lysates from the SOD1-G93A mouse model. NF-κB DNA binding activity was increased in end-stage ALS mice compared to WT littermates (Figure S1A). Supershift EMSA analysis revealed the binding contribution of p65 (Figure S1B). Interestingly, we were unable to show a supershift using antisera against p50, c-Rel, and RelB subunits, which may be more of a limitation of the antibody than the lack of presence of these NF-κB subunits in spinal cords of SOD1-G93A mice. To investigate the extent of p65-mediated classical NF-κB activation in the SOD1-G93A mouse model at different stages of disease, whole lumbar spinal cord protein was analyzed for the transcriptionally active, phosphorylated form of p65 from three SOD1-G93A female mice at the pre-symptomatic stage (pre-sym), disease onset, symptomatic (sym), late-symptomatic (late-sym), and end-stage (ES). We found that as diseased progressed in ALS animals, phospho-p65 levels increased modestly from pre-sym to sym, although fold changes were not statistically significant. However, at late-SYM phospho-p65 levels were 13.7-fold

greater in SOD1-G93A mice compared to WT and 8.7-fold greater than WT at ES (Figure 1A and 1B). In order to determine whether the increase in phospho-p65 levels observed at late-sym stages is statistically different compared to the levels at ES, we analyzed lumbar spinal cord lysates from additional late-sym (n=6) and ES SOD1-G93A mice (n=6), revealing no statistical difference in NF-κB activation between late-sym and ES (Figure S1C and S1D). To determine the contribution of astrocytes to this increase, we isolated primary astrocytes from the spinal cords of WT and SOD1-G93A mice at the late-sym stage. Western blot analysis showed a 4.4-fold increase in phospho-p65 in ALS astrocytes compared to WT (Figure 1C).

NF-κB inhibition in astrocytes does not confer neuroprotection *in vitro* or *in vivo* in the SOD1-G93A mice

To determine the relevance of NF-κB activation to astrocyte-mediated MN death in ALS, we tested NF-κB inhibition in an *in vitro* co-culture model of familial ALS. We utilized an embryonic stem cell line containing an Hb9-GFP reporter, which we and others have shown recapitulate aspects of MN pathology and cell death when co-cultured with ALS glia (Di Giorgio et al., 2007; Haidet-Phillips et al., 2011; Nagai et al., 2007; Wichterle et al., 2002). After 5 days in co-culture, the number of MNs present on SOD1-G93A astrocytes was statistically reduced by 49% compared to the MNs surviving on WT astrocytes (Figure S2A). To test the role of NF-κB in SOD1-G93A astrocytes, we utilized an adenovirus expressing the transdominant super repressor inhibitor of NF-κB (IκBα-SR). IκBα-SR is an IκBα mutant that is resistant to phosphorylation-induced degradation thus blocking phosphorylation sites of p65 and inhibiting transcriptional function of the NF-κB complex (Wang et al., 1999). We confirmed that adenoviral vectors were capable of targeting nearly 100% of astrocytes *in vitro* (data not shown) (Miranda et al., 2012). However, overexpression of IκBα-SR in SOD1-G93A astrocytes did not rescue MN death *in vitro* despite being functional and decreasing phospho-p65 levels (Figure S2A and S2B). In fact, there were less MNs surviving after 4 days in co-culture with SOD1-G93A astrocytes overexpressing IκBα-SR compared to SOD1-G93A astrocytes, however, significance was lost on subsequent days (Figure S2A).

Since our *in vitro* model may not fully recapitulate all aspects of astrocyte-induced pathology in ALS, we simultaneously tested NF-κB inhibition *in vivo* using two independent, cell type-specific approaches: viral-

mediated gene delivery and transgenic cre-lox recombination. As a therapeutically relevant study, we injected SOD1-G93A mice with adeno-associated viral vector serotype 9 (AAV9) to deliver IκBα-SR. Mice were injected at postnatal day 60 to preferentially target >50% astrocytes in the CNS (Foust et al., 2008; 2013). Consistent with the *in vitro* data above, overexpression of IκBα-SR in astrocytes utilizing AAV9 did not alter survival nor improve motor performance in the SOD1-G93A mice compared to non-injected controls (Figure 1D and E) or SOD1-G93A mice injected with AAV9-GFP (Foust 2013).

To transgenically inhibit NF-κB in astrocytes in SOD1-G93A mice, we mated SOD1-G93A mice to mice with conditional mutants of IKKβ (IKKβ$^{f/f}$), which have exon 3 of the *ikbkb* (IKKβ) gene flanked by loxP sites (Li et al., 2003; Park et al., 2002). We crossed these mice to a strain expressing cre recombinase under the regulation of the glial fibrillary acidic protein (GFAP) promoter, thus ablating IKKβ and downstream NF-κB activity specifically in astrocytes. We confirmed cre expression was restricted to GFAP-expressing astrocytes in the spinal cord by crossing GFAP-cre mice to a Rosa26 line that expresses tdTomato (RFP) in all cre-expressing cells (Figure S2C). We observed robust RFP expression in GFAP+ and EAAT2+ cells (Figure S2D); RFP expression was absent in Iba-1+ microglia as well as in ChAT+ neurons in the spinal cord as previously reported (Figure S2C) (Yamanaka et al., 2008; Zhuo et al., 2001). Immunoblot of lumbar spinal cord protein demonstrated a 58% reduction in phospho-p65 levels in SOD1; IKKβ$^{f/f}$; GFAP-cre+ mice compared to SOD1 cre- mice at the symptomatic stage of disease (Figure S2E). Despite the reduction in phospho-p65, motor impairment and survival in the GFAP-cre+ mice were not improved compared to GFAP-cre- negative controls (Figure 1F and 1G). Indeed, our findings are consistent with a recent study crossing ALS mice to a strain overexpressing IκBα-SR under the GFAP promoter (Crosio et al., 2011b).

NF-κB activation occurs predominately in microglia in the SOD1-G93A mouse model

To evaluate whether astrocytes are the main cells contributing to the increase in lumbar NF-κB activation, we crossed the SOD1-G93A mice to a NF-κB-GFP reporter mouse strain that expresses GFP under the control of NF-κB *cis* elements (Magness et al., 2004). Since robust NF-κB activation in SOD1-G93A was evident at late stages of disease in lumbar spinal cord protein, we analyzed lumbar spinal cord sections from late-sym SOD1; NF-κB-GFP mice for GFP expression. We observed a population of bright GFP+ cells

identified as microglia by overlapping confocal Iba-1 staining (Figure 2A). We also observed a dim GFP+ population of GFAP+ astrocytes (Figure 2B). We confirmed these findings by analyzing phospho-p65 levels in protein from microglia isolated from late-sym SOD1-G93A mice. Impressively, phospho-p65 was 12.4 fold greater in SOD1-G93A microglia than WT microglia (Figure 2C). To determine the time course of NF-κB activation in microglia as disease progressed, we performed immunohistochemistry of SOD1; NF-κB-GFP lumbar spinal cord sections at pre-sym, onset, sym, late-sym, and at ES. We observed that majority of bright and dim GFP+ cells co-localized with the microglial marker tomato lectin at disease onset with an increase in the number and GFP intensity as disease progressed, coinciding with microglial activation and gliosis (Figure 2D and 2E). These data reveal that microglia contribute to the robust NF-κB activation that occurs during ALS disease progression.

Adult SOD1-G93A microglia are toxic to MNs *in vitro*

To study the mechanisms by which microglia mediate MN death in ALS and the contribution of NF-κB activation to this process, we sought to establish an *in vitro* co-culture model of ALS. We found no difference in MN survival when MNs were co-cultured with SOD1-G93A primary neonatal microglia compared to WT (Figure S3), suggesting these young cells were not recapitulating important aspects of the adult-onset neurodegenerative disease. Therefore, we established a co-culture utilizing primary adult microglia isolated from symptomatic ALS mice. We utilized a previously described method that combines density separation and culture selection (Moussaud and Draheim, 2010). Immunocytochemical characterization of adult microglia obtained by this method were positive for prototypic microglial markers including Iba-1, CD11b, and F4/80 and negative for GFAP, ChAT, and NG2 (Figure 3A and B). Flow cytometry confirmed that this technique yields a homogenous population of microglia (Figure 3C). We observed no difference in our assays when we used spinal cord or brain-derived microglia, therefore, to decrease the number of animals used, we performed experiments using brain microglia.

To determine the capacity for SOD1-G93A adult microglia to induce MN death, we co-cultured WT Hb9:GFP+ MNs with WT or SOD1-G93A microglia. After 72 hours, MN numbers decreased 50% when co-cultured with SOD1-G93A microglia compared to WT microglia (Figure 3D and 3E). To confirm that MN death

is specific to the causative SOD1 mutation, we overexpressed a shRNA targeting the human SOD1 transgene in the SOD1-G93A microglia by lentivirus, shown to reduce mutant protein by 75% (Figure 3F). When mutant SOD1 protein was reduced in SOD1-G93A microglia, MNs survival was rescued (Figure 3D and 3E).

Adult SOD1-G93A microglia induce MN death in an NF-κB dependent mechanism *in vitro*.

To examine whether NF-κB activation in microglia is involved in MN death *in vitro*, we employed two independent approaches to abolish NF-κB activation in microglia. First, we overexpressed IκBα-SR via adenovirus (Ad-IκBα-SR) in SOD1-G93A and WT microglia. We also employed a genetic approach by isolating microglia from SOD1-G93A; $IKK\beta^{f/f}$ mice and infecting the microglia *in vitro* with an adenovirus expressing cre recombinase (Ad-cre) to remove $IKK\beta^{f/f}$ in microglia post-isolation. After 12 hours, we observed no difference in survival or axon length of the MNs co-cultured with SOD1-G93A or WT microglia (Figure 4A). However, after 72 hours of co-culture there was a 61% reduction in MN survival and marked reduction in axon length when MNs were co-cultured with SOD1-G93A microglia compared to WT (Figure 4B). Live-imaging of these co-cultures captures the dynamic nature of microglia and rapid MN death induced by SOD1-G93A microglia (Movie S1 and S2). Initially, WT microglia phagocytosed MN debris generated from the FACS sorting and plating. Then WT microglia proceeded to actively survey synapses of MNs, not disrupting intact synapses. On the contrary, SOD1-G93A microglia assaulted intact synapses, thus causing axonal damage and MN death, finishing with phagocytosis of the neuronal debris. Remarkably, NF-κB inhibition, either transgenically or by overexpression of IκBα-SR, fully rescued MN axon length and survival *in vitro* to WT levels (Figure 4A and 4B). Live-imaging shows SOD1-G93A microglia with NF-κB inhibition preserved intact MNs similar to WT microglia (Movie S3 and Movie S4). We evaluated the efficiency of NF-κB induction by measuring nitric oxide (NO) and TNF-α levels in the co-culture medium, both of which are products of classical NF-κB activation and inflammatory microglia (Ghosh and Karin, 2002). TNF-α levels decreased by 45% and by 64% when NF-κB was inhibited in SOD1-G93A microglia using Ad-IκBα-SR and Ad-cre, respectively (Figure 4C). Nitric oxide (NO) levels were reduced by 71% and by 56% in SOD1-G93A microglia using Ad-IκBα-SR and Ad-cre, respectively (Figure 4D). Corresponding with TNF-α and NO levels, phospho-p65 was

reduced by 79% and 81% using Ad-IκBα-SR and Ad-cre, respectively, compared to SOD1-G93A microglia (Figure 4E). To confirm NF-κB transcriptional activity was reduced with Ad-IκBα-SR and Ad-cre, we performed an NF-κB luciferase assay. Firefly luciferase activity normalized to renilla luciferase was 6.2-fold greater in SOD1-G93A microglia compared to wild-type and Ad-IκBα-SR and Ad-cre both reduced NF-κB-dependent luciferase activity in SOD1-G93A microglia to near wild-type levels (Figure 4F). These data suggest that SOD1-G93A microglia induce MN death in an NF-κB-dependent mechanism.

SOD1-G93A microglia induce MN death in an NF-κB dependent mechanism *in vivo*.

Since we have established that (1) NF-κB activation during the disease course in SOD1-G93A mice occurs in microglia (Figure 2) and (2) SOD1-G93A microglia kill MNs *in vitro* via an NF-κB-dependent mechanism (Figure 4), we tested the hypothesis that NF-κB inhibition in microglia would attenuate disease in SOD1-G93A mice. To do so, we crossed SOD1-G93A; IKKβ$^{f/f}$ mice to mice expressing cre recombinase driven by the promoter for the gene *c-fms* which encodes Colony Stimulating Factor Receptor 1 (CSF-1R). As shown by MacGreen reporter mice that express GFP under the regulation of the *c-fms* promoter, CSF-1R is expressed throughout the mononuclear phagocyte system of the mouse, but only microglia express CSF-1R in the postnatal mouse brain (Erblich et al., 2011; Sasmono and Williams, 2012; Sasmono et al., 2003). To confirm cell-type specificity of cre expression driven by the *c-fms* (CSF-1R) promoter, we crossed CSF-1R-cre mice to the Rosa26-Td-Tomato mouse strain. We observed RFP expression only in Iba-1-positive microglia in the adult mouse spinal cord, and RFP expression was absent in MNs and astrocytes (Figure S4A and S4B).

Mice homozygous for IKKβ (IKKβ$^{f/f}$), both SOD1 and WT, displayed serious immune dysfunction such as enlarged spleens, eye infections, and missing or very brittle teeth which have been previously reported in mice with myeloid cells devoid of NF-κB (Ruocco et al., 2005; Vallabhapurapu and Karin, 2013). These mice could not be maintained in the colony long enough to evaluate survival, thus, we analyzed IKKβ$^{f/wt}$ heterozygous mice. To determine the efficiency of IKKβ knockdown in these heterozygotes, immunohistochemistry was performed probing for IKKβ in lumbar spinal cord sections from SOD1-G93A; IKKβ$^{f/wt}$; CSF-1R-cre+ and cre- mice. SOD1-G93A; IKKβ$^{f/wt}$; CSF-1R-cre+ showed a decrease in IKKβ

staining compared to cre negative controls (Figure S4C). To ensure knockdown was specific for IKKβ, we evaluated IKKγ, the regulatory subunit of the IKK signaling complex, and observed no difference between CSF-1R-cre+ and cre- mice (Figure S4C). Remarkably, reducing IKKβ, and thus NF-κB activation, resulted in a pronounced 20 day extension in median survival in SOD1-G93A; IKKβ$^{f/wt}$; CSF-1R-cre+ mice compared to cre- controls (133 days in cre- and 153 days in cre+) (Figure 5A). While disease onset was not altered (102.8±1.1 days in cre- and 101.1±1.3 days in cre+), disease progression was significantly extended by 47% in cre+ mice compared to cre- mice (34.8±1.4 days in cre- and 51.1.1±1.7 days in cre+) (Figure 5B and 5C). Video of age-matched littermates show SOD1-G93A; IKKβ$^{f/wt}$; CSF-1R-cre+ mouse able to ambulate around cage while SOD1-G93A; IKKβ$^{f/wt}$; CSF-1R-cre- littermate is at ES (Movie S5). To confirm the level of NF-κB inhibition that was achieved to slow disease progression by 47%, we analyzed lumbar spinal cord protein for phospho-p65 from SOD1-G93A; IKKβ$^{f/wt}$; CSF-1R-cre+ or cre- mice at ES. Remarkably, phospho-p65 was reduced by 44% in SOD1-G93A; IKKβ$^{f/wt}$; CSF-1R-cre+ mice compared to cre- SOD1 controls, which expressed 7.5 fold more phospho-p65 than WT controls. This is consistent with the 40% decrease in IKKβ we observed in SOD1-G93A; IKKβ$^{f/wt}$; CSF-1R-cre+ mice compared to cre- controls (Figure 5D). Notably, NF-κB inhibition did not reduce the levels of mutant SOD1 in CSF-1R-cre+ mice compared to cre- SOD1 control mice (Figure 5D).

To determine the impact of NF-κB inhibition on astrogliosis and microgliosis, we analyzed lumbar spinal cord sections by immunohistochemistry for intensity of GFAP and Iba-1, respectively. No difference in gliosis could be detected between ES SOD1-G93A; IKKβ$^{f/wt}$; CSF-1R-cre+ and cre- mice (data not shown). However, considering that SOD1-G93A; IKKβ$^{f/wt}$; CSF-1R-cre+ endured disease for an additional 3 weeks compared to controls, it is possible that differences in gliosis achieved earlier in disease are lost at ES. Indeed, when we sacrificed the SOD1-G93A; IKKβ$^{f/wt}$; CSF-1R-cre+ mice at the same age as the cre- littermate control reached end-point, we observed a significant decrease in signal intensity of GFAP by 31% and of Iba-1 by 25%, indicating astrogliosis and microgliosis are decreased in CSF-1R-cre+ mice compared to age-matched controls (Figure 5E-5G).

NF-κB regulates SOD1-G93A microglial conversion to an inflammatory, neurotoxic phenotype

We hypothesized that the increased survival observed in SOD1-G93A; IKKβ$^{f/wt}$; CSF-1R-cre+ mice was due to a dampened inflammatory microglial response. To characterize microglia phenotype, antibodies specific for CD68, iNOS, and CD86 were used to label microglia exhibiting an M1 inflammatory phenotype (Kigerl et al., 2009). As disease progresses, we and others have observed SOD1-G93A mice exhibit a robust induction in CD68-positive microglia that is greatest at ES (data not shown) (Beers et al., 2011b; Chiu et al., 2013). We found a marked reduction in the number of CD68 positive microglia in SOD1-G93A; IKKβ$^{f/wt}$; CSF-1R-cre+ mice (112.4 ± 4.7 cells/section) compared to cre-negative controls (438.3 ± 13.4 cells/section) (Figure 6A and 6B). The number of iNOS+/Iba1+ cells/section was also significantly reduced from 251.1 ± 15.0 in controls to 47.8 ± 3.1 in mice with microglial NF-κB inhibition (Figure 6C, 6D). Following the same trend, mice with microglial NF-κB inhibition showed substantial reduction of CD86+/Iba1+ cells (97.8 ± 7.4 per section) compared to SOD1 controls (320.3 ± 15.6 cells per section) (Figure 6E and 6F). We did not observe any alterations in the M2 markers CD206, arginase, CD204 by immunohistochemistry, suggesting that while we inhibited M1 microglia, NF-κB inhibition did not promote an M2 phenotype (data not shown).

NF-κB activation selectively in WT microglia is sufficient to induce MN death *in vitro*

We hypothesized that if NF-κB activation is the mechanism by which SOD1-G93A microglia induce MN death, constitutively activating NF-κB in WT microglia should be sufficient to induce MN death. To test this hypothesis we isolated microglia from Rosa26-Stop^{Flox}IKKβCA mice containing inducible constitutively active IKKβ (IKKβ CA). Post-isolation we infected microglia from these mice with an adenovirus expressing cre recombinase (Ad-cre) to induce transcription of constitutively active IKKβ (microglia termed IKKβCA) or Ad-RFP as control (microglia termed WT). After 12 hours in co-culture with WT or IKKβCA microglia, we observed no difference in MN axon length or survival (Figure 7A). Interestingly, after 72 hours in co-culture IKKβCA microglia induced a 50% statistical decrease in MN survival compared to controls (Figure 7A, 7B). Live-imaging shows IKKβCA microglia rapidly inducing MN death (Movie S6). We confirmed NF-κB activation by ELISA, showing 1.7-fold greater phospho-p65/total p65 in IKKβCA microglia compared to WT (Figure 7C). Similarly, NF-κB-dependent luciferase activity normalized to renilla was 1.5-fold greater in IKKβCA microglia compared to WT (Figure S5A). Additionally, TNF-α levels increased 2.3-fold in co-cultures with IKKβCA

microglia compared to WT, which is comparable to TNF-α induction by SOD1-G93A microglia and characteristic of activated microglia (Figure S5B). Similarly, nitric oxide (NO) levels in IKKβCA microglia/MN co-culture were 1.5 fold greater than WT (Figure S5C). These data suggest that constitutive NF-κB activation in microglia is sufficient to induce MN death independent of SOD1 mutations.

NF-κB regulates microglial activation to an inflammatory, neurotoxic phenotype

Since we observed a reduction in inflammatory microglial markers CD68, iNOS, and CD86 with NF-κB inhibition, we hypothesized that NF-κB is required for microglial activation. Thus, we reasoned that selectively expressing constitutively active IKKβ (IKKβCA) in myeloid cells *in vivo* should induce an inflammatory state in WT microglia similar to that observed in ALS mice. To test this notion, we crossed mice expressing CSF-1R-cre to Rosa26-Stop^{Flox}IKKβCA mice (termed IKKβCA). IKKβCA mice exhibited an 8.2 fold increase in phospho-p65 in lumbar spinal cord protein compared to cre-negative littermates, similar to levels in SOD1-G93A mice (Figure 7D). Enhanced microglial activation at 4 and 8 months in these mice also was associated with pronounced astrocytosis (Figure 7E). By 8 months we observed a striking 40% decrease in ChAT+ MNs in the lumbar spinal cord (Figure 7F) which coincided with decreased mass and hind-limb grip strength in IKKβCA mice compared to WT littermates (Figure 7G and 7H). Thus, chronic activation of NF-κB signaling in myeloid cells creates the pathological features of ALS in the spinal cord, i.e., gliosis and MN death. While we focused on lumbar spinal MNs, it is likely other neurons and brain regions are affected by microglial activation in IKKβCA mice.

To determine whether microglia in IKKβCA mice express activation markers, similar to those described above for activated (M1) microglia from SOD1-G93A mice, we analyzed microglia from the IKKβCA and cre-negative littermates for expression of CD68, iNOS, and CD86. A striking upregulation of CD68 and CD86 was observed in microglia from 4 month and 8 month-old IKKβCA mice (Figure S6A and S6B). Microglia from IKKβCA mice also differed drastically from those found in WT controls exhibiting a de-ramified morphology with shorter, thickened processes shown by Iba-1 staining. We detected an increase in iNOS+ microglia compared to WT controls at 8 months, but not at 4 months in IKKβCA mice (Figure S6C). Interestingly, we observed an

increase in CD68 and CD86-positive microglia in 8 month WT controls compared to 4 month-old controls, which supports previous reports that microglial activation increases with aging (Norden and Godbout, 2013). These data suggest that chronic NF-κB activation induces an inflammatory (M1) microglia phenotype that causes MN death.

DISCUSSION

Landmark studies have shown selective removal of the causal mutant SOD1 gene from myeloid cells in the slow-progressing SOD1-G37R mice (Boillee et al., 2006) or repopulating the fast-progressing SOD1-G93A model with WT myeloid cells, delays disease progression (Beers et al., 2006). Therefore, we hypothesized that if NF-κB activation is a mechanism by which mutant SOD1 microglia mediates MN death in ALS, then disease progression will be substantially delayed in SOD1-G93A mice with microglial NF-κB inhibition. Mice homozygous for IKKβ (IKKβ$^{f/f}$), both SOD1 and WT, displayed serious immune dysfunction and could not be assessed for survival, so we generated SOD1; CSF1R-cre; IKKβ$^{F/+}$ heterozygous mice. Strikingly, heterozygous inhibition of NF-κB specifically in the myeloid lineage of the fast-progressing SOD1-G93A mouse model significantly delayed disease progression by 47% resulting in a 20 day increase in survival. Therefore, our data extend those showing that ALS microglia contribute to MN death in a non-cell autonomous mechanism, and for the first time we report that microglial-mediated MN death in ALS occurs through an NF-κB-dependent mechanism.

To determine the extent by which NF-κB inhibition in microglia alters the neuroinflammatory hallmarks of ALS pathology, we analyzed lumbar sections for astrogliosis, microgliosis and MN death. In SOD1-G93A; IKKβ$^{f/wt}$; CSF1R-cre+ mice with NF-κB inhibition in microglia, we observed a decrease in Iba-1 and GFAP compared to age-matched cre-negative control littermates, suggesting NF-κB inhibition delayed microglial activation and astrogliosis during disease progression. Additionally, we show NF-κB inhibition in astrocytes results in no benefit to ALS mice and in fact might be detrimental, which has been previously reported (Crosio et al., 2011b). It is likely NF-κB might regulate important aspects of astrocyte function that are needed to support MNs under insult in ALS, which may explain why no benefit was observed with astroglial NF-κB

inhibition in SOD1-G93A mice (Beattie et al., 2002; Bracchi-Ricard et al., 2008). These data suggest that astrocytes elicit a different non-cell autonomous mechanism than microglia to induce MN death in ALS.

To determine whether the survival increase observed in SOD1-G93A; IKKβ$^{f/wt}$; CSF-1R-cre+ mice was due to a dampened pro-inflammatory microglial response, we characterized microglia for known markers of microglial activation. Depending on the milieu in which they become activated, microglia differentiate into inflammatory (M1) and anti-inflammatory (M2) effector cells with the potential to kill invading pathogens or neurons (M1), promote tissue repair or dampen the immune response (M2) (Kigerl et al., 2009). These activation states were characterized initially in macrophages *in vitro* and likely represent an oversimplification of the *in vivo* functional potential of these cell types (Mosser and Edwards, 2008; Ransohoff and Perry, 2009). Not surprisingly, ALS microglia have a unique pro-inflammatory (M1) gene signature compared to LPS-stimulated M1 microglia (Chiu et al., 2013). Previous reports showed an upregulation of genes in SOD1-G93A mice known to be expressed by inflammatory (or M1) microglia such as CD68, CD86, iNOS, TNF-α, NOX2, COX2, IL-6, and IL-1β, which increase with disease progression. In fact, SOD1-G93A; IKKβ$^{f/wt}$; CSF-1R-cre+ mice exhibited a marked reduction in prototypic ALS microglia inflammatory markers such as CD68, CD86 and iNOS compared to cre-negative controls, suggesting pro-inflammatory, M1 microglia play a central role in MN death in ALS (Beers et al., 2011a; Henkel et al., 2009; Zhao et al., 2004). Additionally, a recent report suggests infiltrating inflammatory monocytes contribute to MN death in ALS (Butovsky et al., 2012). Since CSF1R-cre is expressed in microglia and peripheral myeloid cells, we cannot exclude the possibility that the delay in disease progression we observe is due to NF-κB inhibition in peripheral macrophages or infiltrating monocytes. To further address the contribution of peripheral myeloid cells to ALS, new cre mouse strains or viral vectors need to be developed that exclusively target microglia or peripheral macrophages/monocytes.

Since NF-κB activation is the mechanism by which SOD1-G93A microglia induce MN death, we hypothesized that constitutively activating NF-κB in WT microglia should be sufficient to induce MN death. Interestingly, microglia with constitutively active NF-κB rapidly induced a 50% decrease in MN survival *in vitro* compared to controls through a mechanism that is independent of mutant SOD1. Notably, 8 month old IKKβCA mice exhibit a marked reduction in spinal MNs, accompanied by reduced weight and grip strength,

indicative of muscle atrophy. While we cannot determine whether microglia or peripheral myeloid cells are inducing MN death, these data have strong implications for patients with familial mutations other than SOD1 and sporadic ALS patients. Recently, immunohistochemical studies showed that NF-κB is highly induced in microglia of sporadic patients and those with mutation in the gene Optinuerin, a negative regulator of TNF-α, induced NF-κB activation that has been shown to cause ALS (Sako et al., 2012). Additionally, TDP-43 and FUS have been shown to be co-activators of NF-κB, and NF-κB inhibition in transgenic mice overexpressing mutant TDP-43 ameliorated the disease phenotype (Swarup et al., 2011; Uranishi et al., 2001). Furthermore, dysregulation of the NF-κB pathway in lymphoblastoid cell lines was identified by MetaCore analysis in both C9ORF72 patients and non-C9ORF72 patients (Ismail et al., 2013). Therefore, aberrant NF-κB activation could be driving the microglial inflammatory response in both familial and sporadic ALS and could be a universal therapeutic target for ALS.

However, targeting NF-κB is complicated due to its diverse functions in different cell types in the CNS and periphery. For example, NF-κB activation in glutamatergic neurons is involved in learning and memory, dendritic arborization, and axonal outgrowth (Gutierrez, 2005; Kaltschmidt et al., 2006). In the context of neurodegeneration, mice with selective inhibition of IKKβ in neuronal cells utilizing a CamkII cre-driver experienced more severe EAE symptoms and succumb to disease earlier due to their inability to induce neuronal expression of NF-κB-dependent neuroprotective and anti-apoptotic genes (Emmanouil et al., 2009; Taoufik et al., 2011). Therefore, when targeting NF-κB in the CNS, cell-type specificity is likely required so that functional benefits achieved by dampening microglial inflammation are not masked by neuronal deficits induced by off-target neuronal NF-κB inhibition (Kaltschmidt and Kaltschmidt, 2009; Mattson and Meffert, 2006).

The data presented here clearly demonstrate that NF-κB is a promising therapeutic target for ALS. Heterozygous inhibition of NF-κB in microglia substantially delayed disease progression in the severe SOD1-G93A model. Strikingly, NF-κB activation in WT microglia causes MN death *in vitro as* well as *in vivo*, independent of mutant SOD1. This suggests traumatic events, environmental risks or pre-disposing genetic

factors that lead to chronic activation of NF-κB in microglia could trigger the pathogenic mechanism leading to MN death. The present data provide important insight on how microglia induce MN degeneration in a familial model of ALS, but even more interestingly, provide a therapeutic target for both familial and sporadic ALS patients.

EXPERIMENTAL PROCEDURES

Transgenic mice

All procedures were performed in accordance with the NIH Guidelines on the care and use of vertebrate animals and approved by the Institutional Animal Care and Use Committee of the Research Institute at Nationwide Children's Hospital. Animals were housed under light:dark (12:12 h) cycle and provided with food and water *ad libitum*. Transgenic female B6SJ/L(SOD1-G93A)1Gur/J mice and non-transgenic littermates (Jackson Laboratories) were utilized for time course immunoblot studies and primary cell isolations. Transgenic male B6SJ/L(SOD1-G93A)1Gur/J mice were used for breeding with other transgenic lines. SOD1 transgene copy number was confirmed by real time PCR. SOD1-G93A-NFκB^{EGFP} reporter mice were generated by breeding SOD1-G93A mice to C57BL/6 NFκB^{EGFP} mice (Christian Jobin) (Magness et al., 2004). SOD1-G93A; hGFAP-cre; IKKβ$^{flox/flox}$ were generated by breeding SOD1-G93A mice to FVB hGFAP-cre (Jackson Labs) mice that had been crossed to C57BL/6 IKKβ$^{flox/flox}$ mice (Li et al., 2003). SOD1-G93A; CSF-1R-icre; IKKβ$^{flox/wt}$ were generated by breeding SOD1-G93A mice to C57BL/6 CSF-1R-cre mice (Deng et al., 2010) that had been bred to IKKβ$^{flox/flox}$ mice. CSF1R-cre; IKKβCA were generated my breeding CSF-1R cre mice to C57BL/6 Rosa26-Stop^{Flox}IKKβCA mice (Jackson Labs). Cre specificity was confirmed by crossing cre lines to C57BL/6 Rosa26-Stop^{Flox}-CAG-tdTomato (Jackson Labs) mice and assessed for tdTomato expression by immunohistochemistry. Genotypes were determined by qualitative PCR using the primers in Supplementary Table 1.

Microglia/MN co-culture

Hb9-GFP+ MNs were plated in 96-well plates coated with laminin (5 μg/ml, Invitrogen) at a density of 6,000 cells per well. The day after microglia were plated on top of MNs at a density of 35,000 cells per well in MN media (DMEM:F12 (Invitrogen), 5% horse serum, 2% N2 (Invitrogen), 2% B27 (Invitrogen) + GDNF (10

ng/ml, Invitrogen), BDNF (10 ng/ml, Invitrogen), CNTF (10 ng/ml, Invitrogen). The co-culture plate was imaged each day by the IN Cell Analyzer 6000 (GE Healthcare). Images were processed and analyzed using IN Cell Developer Toolbox 1.9 and IN Cell Analyzer Workstation 3.7 software (GE Healthcare) to quantify number of surviving GFP+ MNs per well.

Western blot

Cells and tissues were homogenized in Tissue Protein Extraction Reagent (Pierce) with EDTA, Complete protease inhibitor (Roche) and Phospho-STOP (Roche). The samples were run on NuPAGE Novex 4-12% Bis-Tris polyacrilamide gels and transferred to a PVDF membrane (Life Technologies). Blots were blocked in 5% milk powder, 0.5% BSA in PBS-Tween for 1h, and then incubated for overnight at 4°C with primary antibody. Bound primary antibody was detected by horseradish peroxidase conjugated secondary antibody followed by chemiluminescence detection (ECL Western Blot Substrate, Pierce). Antibodies are listed in Supplementary Table 2.

Immunohistochemistry

Animals were deeply anesthetized with a lethal dose of Xylazene/Ketamine and perfused transcardially with saline, then 4% paraformaldehyde. Spinal cords were sectioned 40 μm thick using a vibrating blade microtome (Leica microsystems). Sections were incubated for 2h at room temperature in TBS+ 1% Triton-X + 10% donkey serum. Samples were incubated for 72h at 4°C with primary antibodies, followed by 2h incubation at RT with secondary antibodies. All images were captured on a Zeiss confocal microscope (Carl Zeiss Microscopy, Thornwood, NY, USA). Antibodies are listed in Supplementary Table 2. For quantification of MNs and microglia, lumbar spinal cords were sectioned 40 μm thick from the end of thoracic level 14 to sacral level 1. For MN counts lumbar spinal cord sections were selected every 5th section from the first identifiable L1 section through L6 and sections were selected every 8th section for microglial quantification.

Statistical Analyses

For all statistical tests Graph Pad Prism 6 software (La Jolla, CA) was used. Statistical analyses of mean differences between groups was performed by either Student's t-test, one or two-way ANOVA, followed

by a Bonferroni post hoc analysis depending on the number of variables and time-points in each experiment. All p-values and n values are indicated in figure legends.

Acknowledgements: This work was funded by US National Institutes of Health (NIH) R01 NS644912, Project A.L.S. and Packard Center for ALS Research (P2ALS) and Helping Link Foundation. A.F. is supported by NINDS T32NS077984 Training in Neuromuscular Disease and L.F. is supported by a Marie Curie Fellowship.

REFERENCES

Alexianu, M.E., Kozovska, M., and Appel, S.H. (2001). Immune reactivity in a mouse model of familial ALS correlates with disease progression. Neurology *57*, 1282–1289.

Almer, G., Kikuchi, H., Teismann, P., and Przedborski, S. (2006). Is prostaglandin E(2) a pathogenic factor in amyotrophic lateral sclerosis? Ann Neurol. *59*, 980–983.

Beattie, E.C., Stellwagen, D., Morishita, W., Bresnahan, J.C., Ha, B.K., Zastrow, Von, M., Beattie, M.S., and Malenka, R.C. (2002). Control of synaptic strength by glial TNFalpha. Science *295*, 2282–2285.

Beers, D.R., Henkel, J.S., Xiao, Q., Zhao, W., Wang, J., Yen, A.A., Siklós, L., McKercher, S.R., and Appel, S.H. (2006). Wild-type microglia extend survival in PU.1 knockout mice with familial amyotrophic lateral sclerosis. Proc. Natl. Acad. Sci. U.S.a. *103*, 16021–16026.

Beers, D.R., Henkel, J.S., Zhao, W., Wang, J., Huang, A., Wen, S., Liao, B., and Appel, S.H. (2011a). Endogenous regulatory T lymphocytes ameliorate amyotrophic lateral sclerosis in mice and correlate with disease progression in patients with amyotrophic lateral sclerosis. Brain *134*, 1293–1314.

Beers, D.R., Zhao, W., Liao, B., Kano, O., Wang, J., Huang, A., Appel, S.H., and Henkel, J.S. (2011b). Neuroinflammation modulates distinct regional and temporal clinical responses in ALS mice. Brain Behavior and Immunity *25*, 1025–1035.

Boillee, S., Yamanaka, K., Lobsiger, C.S., Copeland, N.G., Jenkins, N.A., Kassiotis, G., Kollias, G., and Cleveland, D.W. (2006). Onset and progression in inherited ALS determined by motor neurons and microglia. Science *312*, 1389–1392.

Bracchi-Ricard, V., Brambilla, R., Levenson, J., Hu, W.-H., Bramwell, A., Sweatt, J.D., Green, E.J., and Bethea, J.R. (2008). Astroglial nuclear factor-kappaB regulates learning and memory and synaptic plasticity in female mice. J Neurochem *104*, 611–623.

Butovsky, O., Siddiqui, S., Gabriely, G., Lanser, A.J., Dake, B., Murugaiyan, G., Doykan, C.E., Wu, P.M., Gali, R.R., Iyer, L.K., et al. (2012). Modulating inflammatory monocytes with a unique microRNA gene signature ameliorates murine ALS. J. Clin. Invest. *122*, 3063–3087.

Chiu, I.M., Morimoto, E.T.A., Goodarzi, H., Liao, J.T., O'Keeffe, S., Phatnani, H.P., Muratet, M., Carroll, M.C., Levy, S., Tavazoie, S., et al. (2013). A neurodegeneration-specific gene-expression signature of acutely isolated microglia from an amyotrophic lateral sclerosis mouse model. Cell Rep *4*, 385–401.

Clement, A.M., Nguyen, M.D., Roberts, E.A., Garcia, M.L., Boillee, S., Rule, M., McMahon, A.P., Doucette, W., Siwek, D., Ferrante, R.J., et al. (2003). Wild-type nonneuronal cells extend survival of SOD1 mutant motor neurons in ALS mice. Science *302*, 113–117.

Crosio, C., Valle, C., Casciati, A., Iaccarino, C., and Carrì, M.T. (2011a). Astroglial inhibition of NF-κB does not ameliorate disease onset and progression in a mouse model for amyotrophic lateral sclerosis (ALS). PLoS ONE *6*, e17187.

Crosio, C., Valle, C., Casciati, A., Iaccarino, C., and Carrì, M.T. (2011b). Astroglial Inhibition of NF-κB Does Not Ameliorate Disease Onset and Progression in a Mouse Model for Amyotrophic Lateral Sclerosis (ALS). PLoS ONE *6*, e17187.

Deng, L., Zhou, J.-F., Sellers, R.S., Li, J.-F., Nguyen, A.V., Wang, Y., Orlofsky, A., Liu, Q., Hume, D.A., Pollard, J.W., et al. (2010). A novel mouse model of inflammatory bowel disease links mammalian target of rapamycin-dependent hyperproliferation of colonic epithelium to inflammation-associated tumorigenesis. Am. J. Pathol. *176*, 952–967.

Di Giorgio, F.P., Boulting, G.L., Bobrowicz, S., and Eggan, K.C. (2008). Human embryonic stem cell-derived motor neurons are sensitive to the toxic effect of glial cells carrying an ALS-causing mutation. Cell Stem Cell *3*, 637–648.

Di Giorgio, F.P., Carrasco, M.A., Siao, M.C., Maniatis, T., and Eggan, K. (2007). Non–cell autonomous effect of glia on motor neurons in an embryonic stem cell–based ALS model. Nat Neurosci *10*, 608–614.

Emmanouil, M., Taoufik, E., Tseveleki, V., Vamvakas, S.-S., Tselios, T., Karin, M., Lassmann, H., and Probert, L. (2009). Neuronal I kappa B kinase beta protects mice from autoimmune encephalomyelitis by mediating neuroprotective and immunosuppressive effects in the central nervous system. The Journal of Immunology *183*, 7877–7889.

Erblich, B., Zhu, L., Etgen, A.M., Dobrenis, K., and Pollard, J.W. (2011). Absence of colony stimulation factor-1 receptor results in loss of microglia, disrupted brain development and olfactory deficits. PLoS ONE *6*, e26317.

Foust, K.D., Nurre, E., Montgomery, C.L., Hernandez, A., Chan, C.M., and Kaspar, B.K. (2008). Intravascular AAV9 preferentially targets neonatal neurons and adult astrocytes. Nat Biotechnol *27*, 59–65.

Foust, K.D., Salazar, D.L., Likhite, S., Ferraiuolo, L., Ditsworth, D., Ilieva, H., Meyer, K., Schmelzer, L., Braun, L., Cleveland, D.W., et al. (2013). Therapeutic AAV9-mediated Suppression of Mutant SOD1 Slows Disease Progression and Extends Survival in Models of Inherited ALS. Molecular Therapy.

Ghosh, S., and Karin, M. (2002). Missing pieces in the NF-kappaB puzzle. Cell *109 Suppl*, S81–S96.

Gowing, G., Dequen, F., Soucy, G., and Julien, J.-P. (2006). Absence of tumor necrosis factor-alpha does not affect motor neuron disease caused by superoxide dismutase 1 mutations. Journal of Neuroscience *26*, 11397–11402.

Gutierrez, H. (2005). NF- B signalling regulates the growth of neural processes in the developing PNS and CNS. Development *132*, 1713–1726.

Haidet-Phillips, A.M., Hester, M.E., Miranda, C.J., Meyer, K., Braun, L., Frakes, A., Song, S., Likhite, S., Murtha, M.J., Foust, K.D., et al. (2011). Astrocytes from familial and sporadic ALS patients are toxic to motor neurons. Nat Biotechnol *29*, 824–828.

Hall, E.D., Oostveen, J.A., and Gurney, M.E. (1998). Relationship of microglial and astrocytic activation to

disease onset and progression in a transgenic model of familial ALS. Glia *23*, 249–256.

Hayden, M.S., and Ghosh, S. (2008). Shared principles in NF-kappaB signaling. Cell *132*, 344–362.

Henkel, J.S., Beers, D.R., Zhao, W., and Appel, S.H. (2009). Microglia in ALS: the good, the bad, and the resting. J Neuroimmune Pharmacol *4*, 389–398.

Ismail, A., Cooper-Knock, J., Highley, J.R., Milano, A., Kirby, J., Goodall, E., Lowe, J., Scott, I., Constantinescu, C.S., Walters, S.J., et al. (2013). Concurrence of multiple sclerosis and amyotrophic lateral sclerosis in patients with hexanucleotide repeat expansions of C9ORF72. Journal of Neurology, Neurosurgery & Psychiatry *84*, 79–87.

Kaltschmidt, B., and Kaltschmidt, C. (2009). NF-kappaB in the nervous system. Cold Spring Harb Perspect Biol *1*, a001271.

Kaltschmidt, B., Ndiaye, D., Korte, M., Pothion, S., Arbibe, L., Prüllage, M., Pfeiffer, J., Lindecke, A., Staiger, V., Israël, A., et al. (2006). NF-kappaB regulates spatial memory formation and synaptic plasticity through protein kinase A/CREB signaling. Molecular and Cellular Biology *26*, 2936–2946.

Kawamata, T., Akiyama, H., Yamada, T., and McGeer, P.L. (1992). Immunologic reactions in amyotrophic lateral sclerosis brain and spinal cord tissue. Am. J. Pathol. *140*, 691–707.

Kigerl, K.A., Gensel, J.C., Ankeny, D.P., Alexander, J.K., Donnelly, D.J., and Popovich, P.G. (2009). Identification of two distinct macrophage subsets with divergent effects causing either neurotoxicity or regeneration in the injured mouse spinal cord. Journal of Neuroscience *29*, 13435–13444.

Lerman, B.J., Hoffman, E.P., Sutherland, M.L., Bouri, K., Hsu, D.K., Liu, F.-T., Rothstein, J.D., and Knoblach, S.M. (2012). Deletion of galectin-3 exacerbates microglial activation and accelerates disease progression and demise in a SOD1(G93A) mouse model of amyotrophic lateral sclerosis. Brain Behav *2*, 563–575.

Li, Z.-W., Omori, S.A., Labuda, T., Karin, M., and Rickert, R.C. (2003). IKK beta is required for peripheral B cell survival and proliferation. J. Immunol. *170*, 4630–4637.

Magness, S.T., Jijon, H., van Houten Fisher, N., Sharpless, N.E., Brenner, D.A., and Jobin, C. (2004). In vivo pattern of lipopolysaccharide and anti-CD3-induced NF-kappa B activation using a novel gene-targeted enhanced GFP reporter gene mouse. J. Immunol. *173*, 1561–1570.

Mantovani, S., Garbelli, S., Pasini, A., Alimonti, D., Perotti, C., Melazzini, M., Bendotti, C., and Mora, G. (2009). Immune system alterations in sporadic amyotrophic lateral sclerosis patients suggest an ongoing neuroinflammatory process. Journal of Neuroimmunology *210*, 73–79.

Marchetto, M.C.N., Muotri, A.R., Mu, Y., Smith, A.M., Cezar, G.G., and Gage, F.H. (2008). Non-cell-autonomous effect of human SOD1 G37R astrocytes on motor neurons derived from human embryonic stem cells. Cell Stem Cell *3*, 649–657.

Maruyama, H., Morino, H., Ito, H., Izumi, Y., Kato, H., Watanabe, Y., Kinoshita, Y., Kamada, M., Nodera, H., Suzuki, H., et al. (2011). Mutations of optineurin in amyotrophic lateral sclerosis. Nature *465*, 223–226.

Mattson, M.P., and Meffert, M.K. (2006). Roles for NF-κB in nerve cell survival, plasticity, and disease. Cell Death and Differentiation *13*, 852–860.

Miranda, C.J., Braun, L., Jiang, Y., Hester, M.E., Zhang, L., Riolo, M., Wang, H., Rao, M., Altura, R.A., and Kaspar, B.K. (2012). Aging brain microenvironment decreases hippocampal neurogenesis through Wnt-

mediated survivin signaling. Aging Cell *11*, 542–552.

Mosser, D.M., and Edwards, J.P. (2008). Exploring the full spectrum ofmacrophage activation. Nature Reviews Immunology *8*, 958–969.

Moussaud, S., and Draheim, H.J. (2010). A new method to isolate microglia from adult mice and culture them for an extended period of time. Journal of Neuroscience Methods *187*, 243–253.

Nagai, M., Re, D.B., Nagata, T., Chalazonitis, A., Jessell, T.M., Wichterle, H., and Przedborski, S. (2007). Astrocytes expressing ALS-linked mutated SOD1 release factors selectively toxic to motor neurons. Nat Neurosci *10*, 615–622.

Nguyen, M.D., Julien, J.P., and Rivest, S. (2001). Induction of proinflammatory molecules in mice with amyotrophic lateral sclerosis: no requirement for proapoptotic interleukin-1beta in neurodegeneration. Ann Neurol. *50*, 630–639.

Norden, D.M., and Godbout, J.P. (2013). Review: Microglia of the aged brain: primed to be activated and resistant to regulation. Neuropathol Appl Neurobiol *39*, 19–34.

Park, J.M., Greten, F.R., Li, Z.-W., and Karin, M. (2002). Macrophage apoptosis by anthrax lethal factor through p38 MAP kinase inhibition. Science *297*, 2048–2051.

Philips, T., and Robberecht, W. (2011). Neuroinflammation in amyotrophic lateral sclerosis: role of glial activation in motor neuron disease. Lancet Neurol *10*, 253–263.

Ransohoff, R.M., and Perry, V.H. (2009). Microglial physiology: unique stimuli, specialized responses. Annu. Rev. Immunol. *27*, 119–145.

Rosen, D.R., Siddique, T., Patterson, D., Figlewicz, D.A., Sapp, P., Hentati, A., Donaldson, D., Goto, J., O'Regan, J.P., and Deng, H.X. (1993). Mutations in Cu/Zn superoxide dismutase gene are associated with familial amyotrophic lateral sclerosis. Nature *362*, 59–62.

Ruocco, M.G., Maeda, S., Park, J.M., Lawrence, T., Hsu, L.-C., Cao, Y., Schett, G., Wagner, E.F., and Karin, M. (2005). IkappaB kinase (IKK)beta, but not IKKalpha, is a critical mediator of osteoclast survival and is required for inflammation-induced bone loss. J. Exp. Med. *201*, 1677–1687.

Sako, W., Ito, H., Yoshida, M., Koizumi, H., Kamada, M., Fujita, K., Hashizume, Y., Izumi, Y., and Kaji, R. (2012). Nuclear factor κ B expression in patients with sporadic amyotrophic lateral sclerosis and hereditary amyotrophic lateral sclerosis with optineurin mutations. Clin. Neuropathol. *31*, 418–423.

Sasmono, R.T., and Williams, E. (2012). Generation and characterization of MacGreen mice, the Cfs1r-EGFP transgenic mice. Methods Mol. Biol. *844*, 157–176.

Sasmono, R.T., Oceandy, D., Pollard, J.W., Tong, W., Pavli, P., Wainwright, B.J., Ostrowski, M.C., Himes, S.R., and Hume, D.A. (2003). A macrophage colony-stimulating factor receptor-green fluorescent protein transgene is expressed throughout the mononuclear phagocyte system of the mouse. Blood *101*, 1155–1163.

Son, M., Fathallah-Shaykh, H.M., and Elliott, J.L. (2001). Survival in a transgenic model of FALS is independent of iNOS expression. Ann Neurol. *50*, 273.

Swarup, V., Phaneuf, D., Dupré, N., Petri, S., Strong, M., Kriz, J., and Julien, J.-P. (2011). Deregulation of TDP-43 in amyotrophic lateral sclerosis triggers nuclear factor κB-mediated pathogenic pathways. Journal of Experimental Medicine *208*, 2429–2447.

Taoufik, E., Tseveleki, V., Chu, S.Y., Tselios, T., Karin, M., Lassmann, H., Szymkowski, D.E., and Probert, L. (2011). Transmembrane tumour necrosis factor is neuroprotective and regulates experimental autoimmune encephalomyelitis via neuronal nuclear factor-kappaB. Brain *134*, 2722–2735.

Turner, M.R., Cagnin, A., Turkheimer, F.E., Miller, C.C.J., Shaw, C.E., Brooks, D.J., Leigh, P.N., and Banati, R.B. (2004). Evidence of widespread cerebral microglial activation in amyotrophic lateral sclerosis: an [11C](R)-PK11195 positron emission tomography study. Neurobiology of Disease *15*, 601–609.

Uranishi, H., Tetsuka, T., Yamashita, M., Asamitsu, K., Shimizu, M., Itoh, M., and Okamoto, T. (2001). Involvement of the pro-oncoprotein TLS (translocated in liposarcoma) in nuclear factor-kappa B p65-mediated transcription as a coactivator. J. Biol. Chem. *276*, 13395–13401.

Vallabhapurapu, S., and Karin, M. (2013). Regulation and function of NF-kappaB transcription factors in the immune system. Annu. Rev. Immunol. *27*, 693–733.

Wang, C.Y., Cusack, J.C., Liu, R., and Baldwin, A.S. (1999). Control of inducible chemoresistance: enhanced anti-tumor therapy through increased apoptosis by inhibition of NF-kappaB. Nat Med *5*, 412–417.

Wichterle, H., Lieberam, I., Porter, J.A., and Jessell, T.M. (2002). Directed differentiation of embryonic stem cells into motor neurons. Cell *110*, 385–397.

Xiao, Q., Zhao, W., Beers, D.R., Yen, A.A., Xie, W., Henkel, J.S., and Appel, S.H. (2007). Mutant SOD1 G93Amicroglia are more neurotoxic relative to wild-type microglia. J Neurochem *102*, 2008–2019.

Yamanaka, K., Chun, S.J., Boillee, S., Fujimori-Tonou, N., Yamashita, H., Gutmann, D.H., Takahashi, R., Misawa, H., and Cleveland, D.W. (2008). Astrocytes as determinants of disease progression in inherited amyotrophic lateral sclerosis. Nat Neurosci *11*, 251–253.

Zhao, W., Xie, W., Le, W., Beers, D.R., He, Y., Henkel, J.S., Simpson, E.P., Yen, A.A., Xiao, Q., and Appel, S.H. (2004). Activated microglia initiate motor neuron injury by a nitric oxide and glutamate-mediated mechanism. J. Neuropathol. Exp. Neurol. *63*, 964–977.

Zhuo, L., Theis, M., Alvarez-Maya, I., Brenner, M., Willecke, K., and Messing, A. (2001). hGFAP-cre transgenic mice for manipulation of glial and neuronal function in vivo. Genesis *31*, 85–94.

FIGURE LEGENDS

Figure 1. The classical NF-κB pathway is activated with disease progression in the SOD1-G93A mouse model and astroglial NF-κB inhibition does not confer neuroprotection.

(A and B) Immunoblot (A) and fold changes (B) of lumbar spinal cord protein isolated from WT mice at 120 days and from SOD1-G93A female mice at pre-symptomatic (Pre), onset (Ons), symptomatic (Sym), late-symptomatic (LSym), and end-stage (ES). phospho-p65 (top) total p65 (middle) and Actin (bottom). n=3. Additional data shown in Supplemental Figure S1.

(C) Immunoblot of protein isolated from astrocytes obtained from late-sym SOD1-G93A and WT littermates.

(D and E) Kaplan-Meier survival curve (D) of SOD1-G93A mice injected with AAV9-IκBα-SR (median survival=128, n=16) and non-injected controls (median survival=136.5, n=14) and motor performance on accelerating rotarod test (E).

(F and G) Kaplan-Meier survival curve (F) of SOD1-G93A; $IKK\beta^{f/f}$; GFAP-cre- (median survival=154, n=10) and SOD1-G93A; $IKK\beta^{f/f}$; GFAP-cre+ mice (median survival=149, n=14) and motor performance on accelerating rotarod test (G).

All band intensities were normalized to p65/Actin.

Error bars represent s.e.m. *, P<0.05, **, P<0.01.

Figure 2. NF-κB activation occurs predominately in microglia in the SOD1-G93A mouse model

(A and B) Representative high magnification images of NF-κB-GFP-positive cells (green) in the lumbar ventral horn of late-symptomatic NF-κB ^{EGFP};SOD1-G93A mice. Most predominant GFP+ cells (A) also positive for microglial marker Iba1+ (red). Other GFP+ cells positive for astrocyte maker GFAP (blue) Scale bar = 5 microns (A) 20 microns (B).

C) Immunoblot of protein isolated from primary microglia obtained from late-sym SOD1-G93A mice and WT littermates. Fold change determined by phospho-p65 band intensity normalized to p65/Actin.

(D) Immunohistochemistry of lumbar ventral horn of WT; NF-κB -GFP at 120 days, and SOD1-G93A; NF-κB -GFP mice pre-sym, onset, sym, late-sym, and ES. NF-κB activation shown by NF-κB ^{EGFP} (green) and microglia and vasculature shown by tomato lectin (red). Scale bar= 50 microns.

(E) Quantification of GFP+ cells co-localizing with tomato lectin in lumbar spinal cord sections of SOD1-G93A; NF-κB -GFP mice.

Error bars represent s.e.m. **, P<0.01, ****, P< 0.0001

Figure 3. Adult SOD1-G93A microglia are toxic to MNs *in vitro*

(A and B) Immunocytochemistry of WT and SOD1-G93A microglia for prototypic microglial markers Iba-1, CD11b, F4/80, and astrocytes (GFAP), oligodendrocyte precursors (NG2), and MNs (ChAT). Quantification per well (B). DAPI (blue) Scale bar = 20 microns.

(C) Flow cytometry of adult microglia for CD45 and CD11b.

(D and E) Representative microscopic field (D) and quantification of well (E) of surviving Hb9-GFP+ MNs after 3 days (72 hours) of co-culture with either WT or SOD1-G93A microglia that were not infected (black bars) or infected with Lv-RFP (dashed bars) or Lv-shRNA-SOD1 (white bars). Scale bar = 200 microns

(F) Quantification of human SOD1 protein in SOD1-G93A microglia infected with Lv-RFP and Lv-shRNA-SOD1 determined by ELISA.

Error bars represent s.e.m. ***, P< 0.001, ****, P<0.0001

Figure 4. Adult SOD1-G93A microglia induce MN death in an NF-κB dependent mechanism *in vitro*.

(A and B) Representative microscopic fields (A) and well counts (B) of Hb9-GFP+ MNs after 1 day (24 hours) and 3 days (72 hours) in co-culture with WT or SOD1-G93A microglia not infected (black bars), infected with Ad-RFP (dashed bars) or Ad-IκBα-SR (white bars). MNs co-cultured with either WT; IKKβ$^{f/f}$ or SOD1-G93A; IKKβ$^{f/f}$ microglia infected with Ad-cre shown with dashed bars. Scale bar = 200 microns

(C and D) Quantification of TNF-α (C) and nitric oxide (D) in the co-culture medium by ELISA.

(E) Quantification of phospho-p65 by ELISA from microglial-MN co-cultures. Phospho-p65 normalized to total p65 determined by ELISA.

(F) Luciferase assay of NF-κB activity in microglia. Firefly luciferase normalized to renilla luciferase.

Error bars represent s.e.m. ****, P< 0.0001, ***, P< 0.001

Figure 5. SOD1-G93A microglia induce MN death in an NF-κB dependent mechanism *in vivo*.

(A) Kaplan-Meier survival curve of SOD1-G93A; IKKβ$^{F/wt}$; CSF1R-cre- (n=22) and SOD1-G93A; IKKβ$^{F/wt}$; CSF-1R-cre+ mice (n=25). Median survival SOD1-G93A; IKKβ$^{F/wt}$; CSF1R-cre- = 133 days, SOD1-G93A; IKKβ$^{F/wt}$; CSF-1R-cre+=153 days. Mean survival SOD1-G93A; IKKβ$^{F/wt}$; CSF1R-cre- =134.9±1.4 days, , SOD1-G93A; IKKβ$^{F/wt}$; CSF-1R-cre+=153.7±0.9 days, P<.0001

(B) Disease onset determined by age at which peak weight was reached. SOD1-G93A; IKKβ$^{F/wt}$; CSF1R-cre- reached onset at 102.8±1.1 days and SOD1-G93A; IKKβ$^{F/wt}$; CSF1R-cre+ mice reached onset at 101.1±1.3 days.
(C) Disease progression defined as time from disease onset to ES. SOD1-G93A; IKKβ$^{F/wt}$; CSF1R-cre- mean disease progression = 34.8±1.4 days and SOD1-G93A; IKKβ$^{F/wt}$; CSF1R-cre+ mean disease progression = 51.1±1.7 days.
(D) Immunoblot of lumbar spinal cord protein isolated from WT; IKKβ$^{F/wt}$; CSF1R-cre+, WT; IKKβ$^{F/wt;}$ CSF1R-cre-, and ES SOD1-G93A; IKKβ$^{F/wt}$; CSF1R-cre-, SOD1-G93A; IKKβ$^{F/wt}$ CSF1R-cre+ mice probed for phospho-p65 (top), total p65, IKKβ, human SOD1 and Actin (bottom). Fold change represents band intensities of phospho-p65 normalized to p65/Actin and IKKβ normalized to Actin.
(E) Immunohistochemistry of Iba1-positive microglia (red) and GFAP-positive astrocytes (green) in the lumbar spinal cords of ES SOD1-G93A; IKKβ$^{F/wt}$ CSF1R-cre-, and age-matched SOD1-G93A; IKKβf$^{/wt}$ CSF1R-cre+, and WT IKKβ$^{f/wt}$ CSF1R-cre+ littermates. Scale bar = 200 microns
(F and G) Quantification of GFAP and Iba-1 signal intensity in SOD1-G93A; IKKβ$^{F/wt}$ CSF1R-cre- and age-matched SOD1-G93A; IKKβ$^{f/wt}$ CSF1R-cre+ immunohistochemistry in represented in (E).

Figure 6. NF-κB inhibition in SOD1-G93A microglia impairs microglial activation to a pro-inflammatory, neurotoxic phenotype

(A and B) Immunohistochemistry (A) and quantification (B) of CD68 (red) and Iba1 (green) cells in lumbar spinal cord of disease-matched ES SOD1-G93A; IKKβ$^{F/wt}$ CSF1R-cre- and SOD1-G93A; IKKβ$^{F/wt}$ CSF1R-cre+ littermates. Scale bar = 200 microns
(C and D) Immunohistochemistry (C) and quantification (D) of iNOS (red) and Iba1 (green) cells in lumbar spinal cord of disease-matched ES SOD1-G93A; IKKβ$^{F/wt}$ CSF1R-cre- and SOD1-G93A; IKKβ$^{F/wt}$ CSF1R-cre+ littermates. Scale bar = 20 microns
(E and F)Immunohistochemistry (E) and quantification (F) of CD86 (red) and Iba1 (green) cells in lumbar spinal cord of disease-matched ES SOD1-G93A; IKKβ$^{F/wt}$ CSF1R-cre- and SOD1-G93A; IKKβ$^{F/wt}$ CSF1R-cre+ littermates. Scale bar = 20 microns

Figure 7. NF-κB activation in wild-type microglia induces MN death

(A and B) Representative microscopic fields (A) and counts (B) of Hb9-GFP+ MNs after 1 day (24 hours) and 3 days (72 hours) in co-culture with WT microglia (white bar) or WT microglia with constitutively active IKKβ (IKKβCA) (black bar).
(C) Quantification of NF-κB activation (phospho-p65), normalized to total p65, both determined by ELISA.
(D) Immunoblot of lumbar spinal cord protein from WT and IKKβCA mice. The blot was probed for p-p65 (top), IKKβ (top middle), p65 (bottom middle) and Actin (bottom). p-p65 band intensities normalized to p65/Actin. Fold change determined by densitometry in Image J.
(E) Immunohistochemistry of lumbar spinal cords of WT and IKKβCA littermates at 8 months. Iba1-positive microglia (red), GFAP-positive astrocytes (blue), ChAT-positive MNs (green). Scale bar = 100 microns
(F) Counts of ChAT+ MNs in ventral horn of lumbar spinal cord from 8-month old IKKβCA and WT littermates. (n=3)
(G and H) Mass (G) and grip strength (H) of IKKβCA (n=6) and WT littermates (n=8).

Figure 8. The classical NF-κB pathway mediates microglial activation and MN death.

(A) Model of the mechanism by which SOD1-G93A microglia induce MN death in ALS. The NF-κB pathway is initiated in SOD1-G93A microglia by a SOD1-G93A-dependent mechanism leading to microglial activation and subsequently, MN death via inflammatory pathways. Inhibition of microglial NF-κB in ALS mice blocks microglial activation, down-regulates pro-inflammatory markers, and delays MN death.
(B) Model of IKKβCA mice in which NF-κB is constitutively active only in myeloid cells. Microglia in these mice exhibit a pro-inflammatory phenotype which induces MN death in a mutant SOD1-independent mechanism.

FIGURE 1

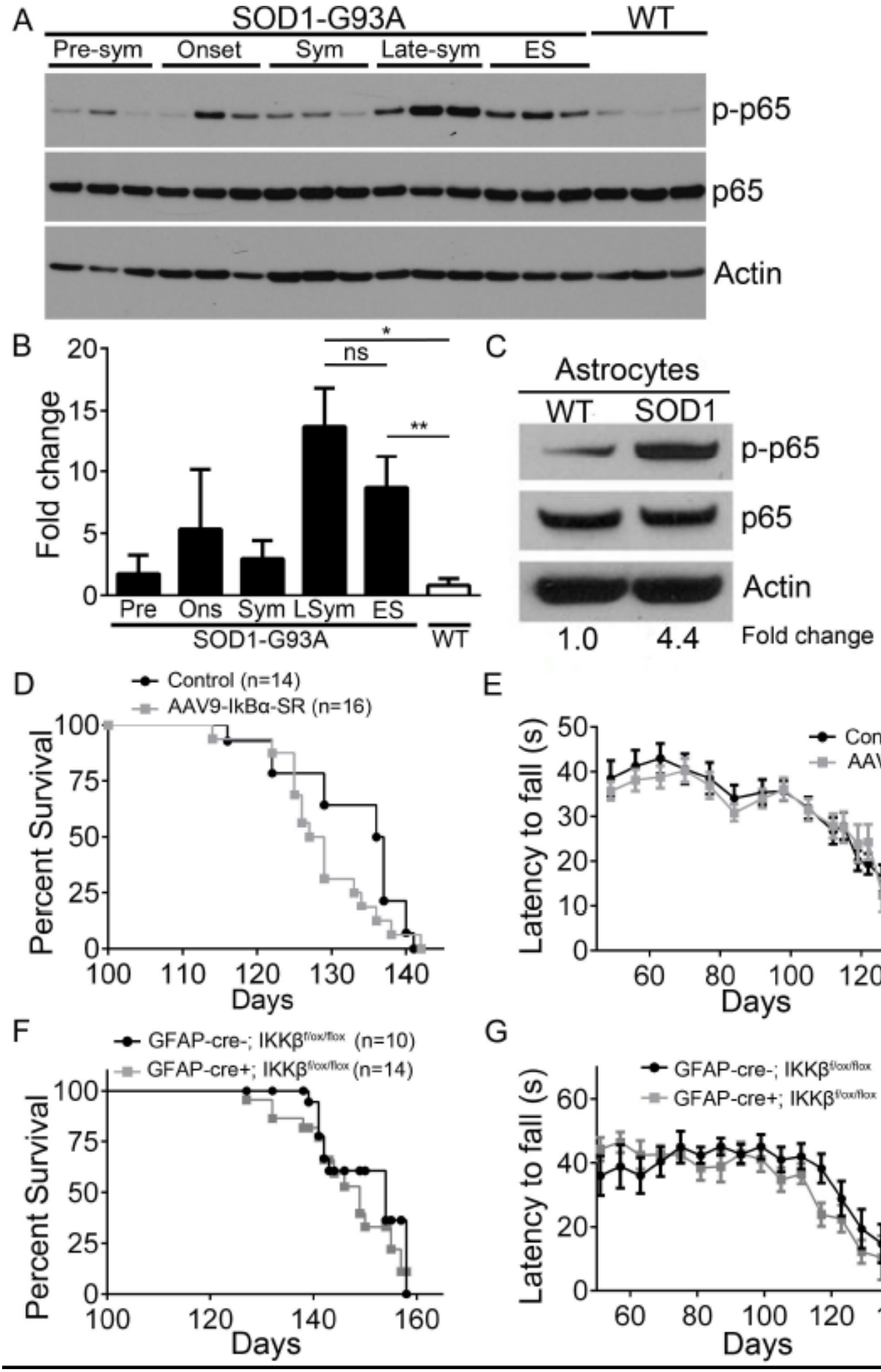
A
SOD1-G93A
WT
Pre-sym
Onset
Sym
Late-sym
ES
p-p65
p65
Actin
B
Fold change
20
15
10
5
0
*
ns
**
Pre
Ons
Sym
LSym
ES
SOD1-G93A
WT
C
Astrocytes
WT
SOD1
p-p65
p65
Actin
1.0
4.4
Fold change
D
Control (n=14)
AAV9-IkBα-SR (n=16)
Percent Survival
100
75
50
25
0
100
110
120
130
140
Days
E
Latency to fall (s)
50
40
30
20
10
0
Control
AAV9-IkBα-SR
60
80
100
120
140
Days
F
GFAP-cre-; IKKβ$^{f/ox/flox}$ (n=10)
GFAP-cre+; IKKβ$^{f/ox/flox}$ (n=14)
Percent Survival
100
75
50
25
0
100
120
140
160
Days
G
Latency to fall (s)
60
40
20
0
GFAP-cre-; IKKβ$^{f/ox/flox}$
GFAP-cre+; IKKβ$^{f/ox/flox}$
60
80
100
120
140
Days

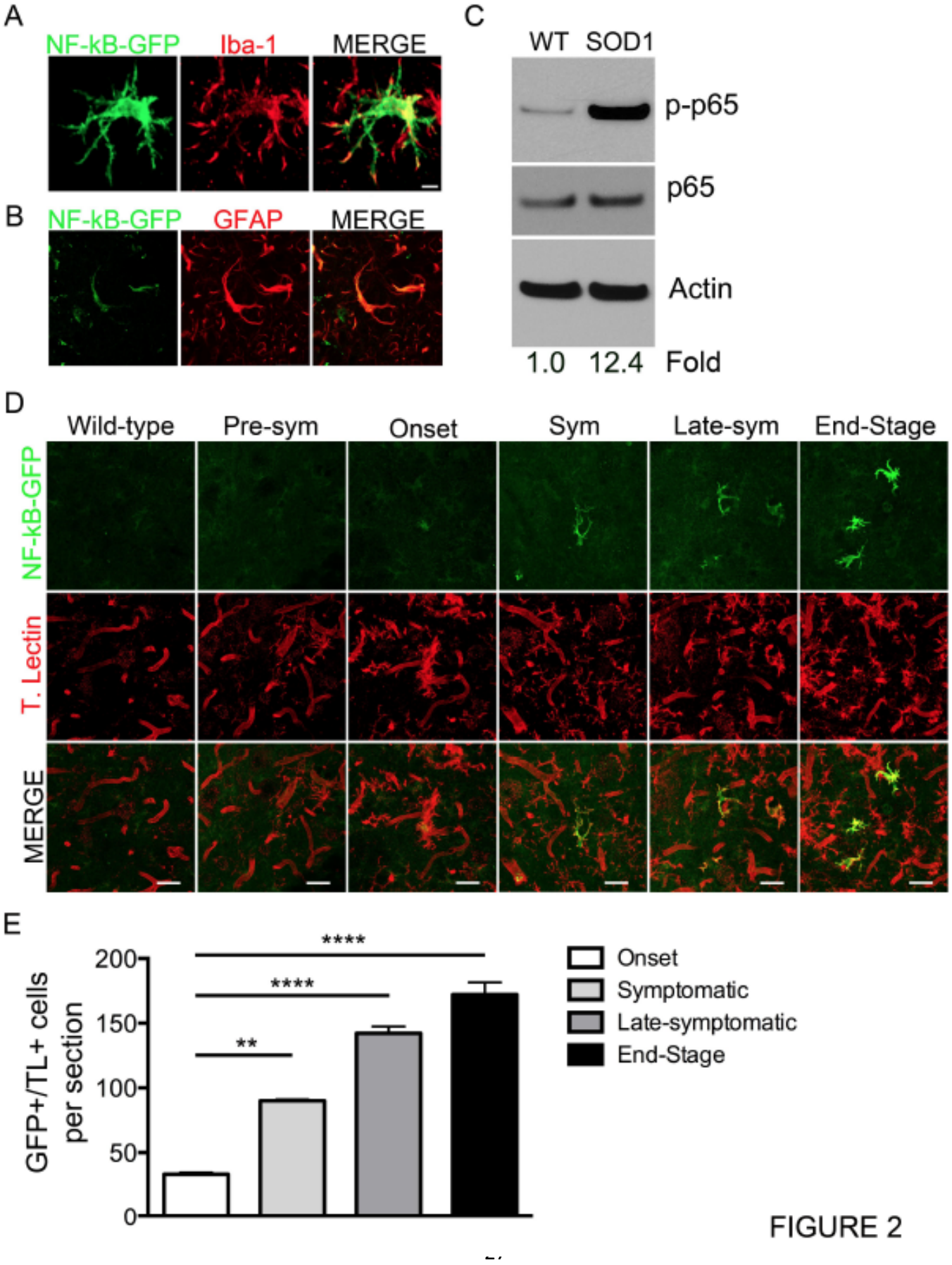
A
NF-kB-GFP
Iba-1
MERGE
B
NF-kB-GFP
GFAP
MERGE
C
WT
SOD1
p-p65
p65
Actin
1.0
12.4
Fold
D
Wild-type
Pre-sym
Onset
Sym
Late-sym
End-Stage
NF-kB-GFP
T. Lectin
MERGE
E
GFP+/TL+ cells per section
200
150
100
50
0
****
****
**
Onset
Symptomatic
Late-symptomatic
End-Stage

FIGURE 2

FIGURE 3

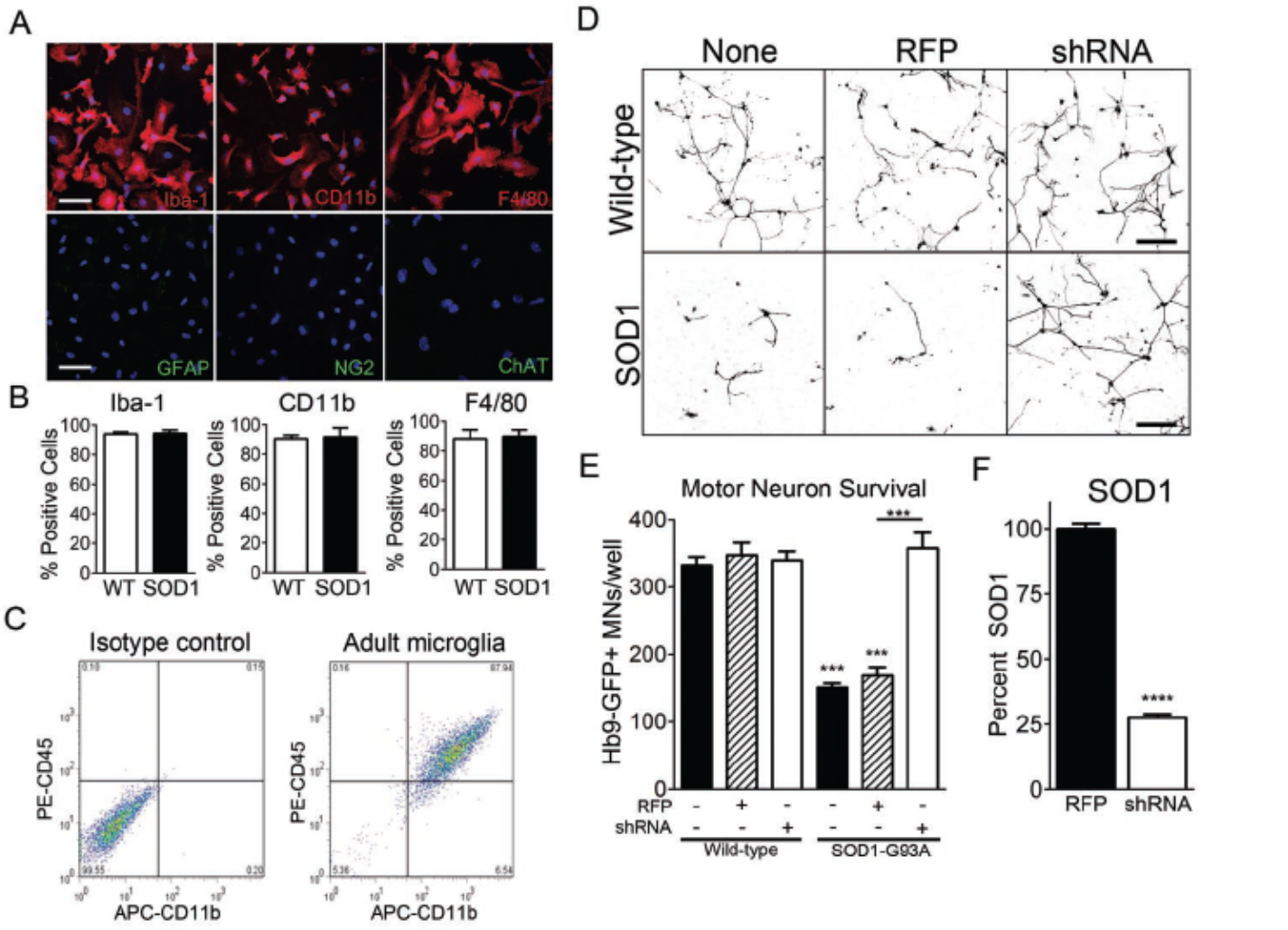
A
Iba-1
CD11b
F4/80
GFAP
NG2
ChAT
B
Iba-1
CD11b
F4/80
% Positive Cells
WT SOD1
C
Isotype control
Adult microglia
PE-CD45
APC-CD11b
D
None
RFP
shRNA
Wild-type
SOD1
E
Motor Neuron Survival
Hb9-GFP+ MNs/well
RFP
shRNA
Wild-type
SOD1-G93A
F
SOD1
Percent SOD1
RFP
shRNA

Figure 4

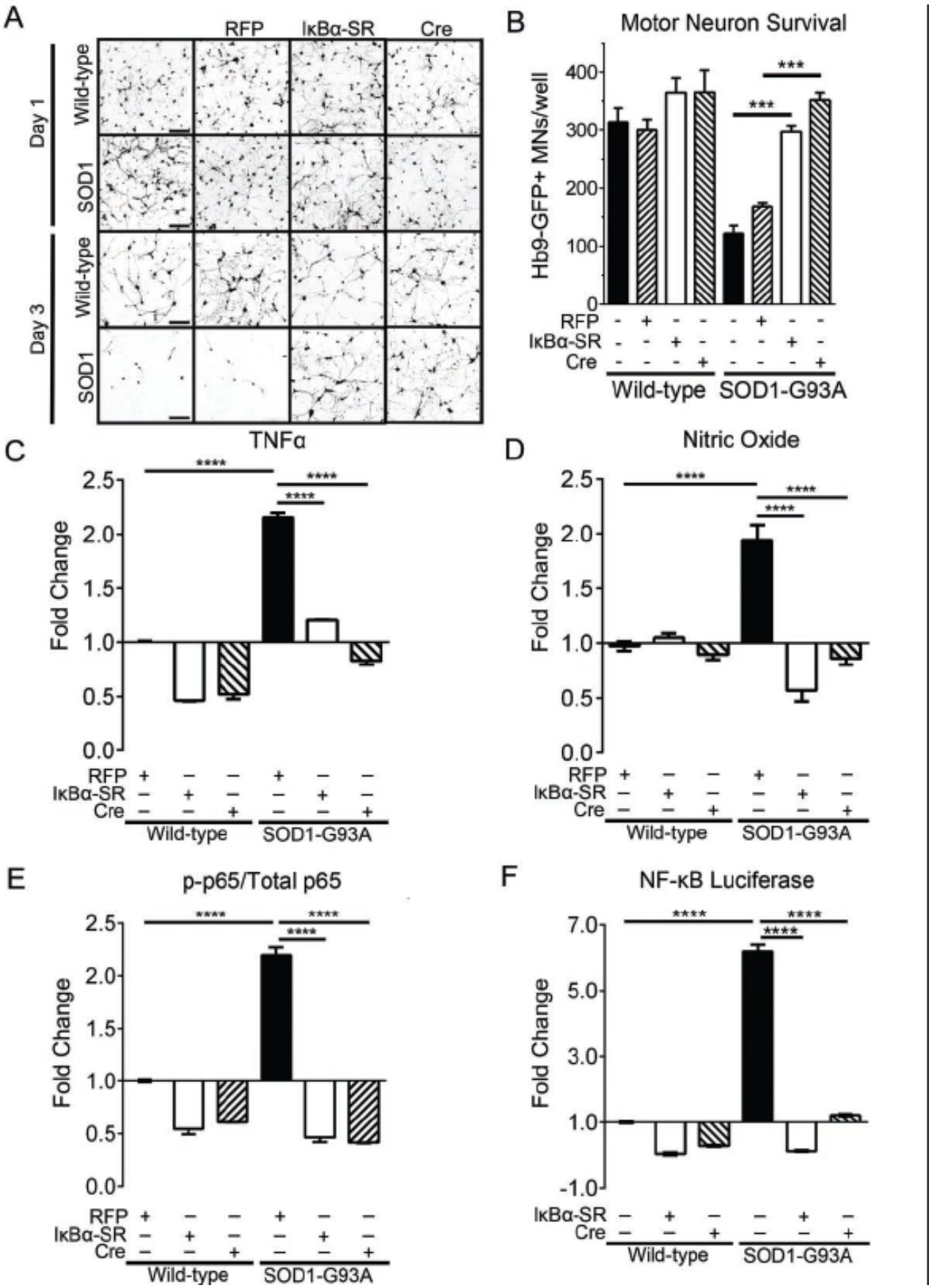
A
RFP
IκBα-SR
Cre
Day 1
Day 3
Wild-type
SOD1
B
Motor Neuron Survival
Hb9-GFP+ MNs/well
400
300
200
100
0
***
***
RFP
IκBα-SR
Cre
Wild-type
SOD1-G93A
C
TNFα
Fold Change
2.5
2.0
1.5
1.0
0.5
0.0
****
****
****
D
Nitric Oxide
E
p-p65/Total p65
F
NF-κB Luciferase
7.0
5.0
3.0
1.0
-1.0

FIGURE 5

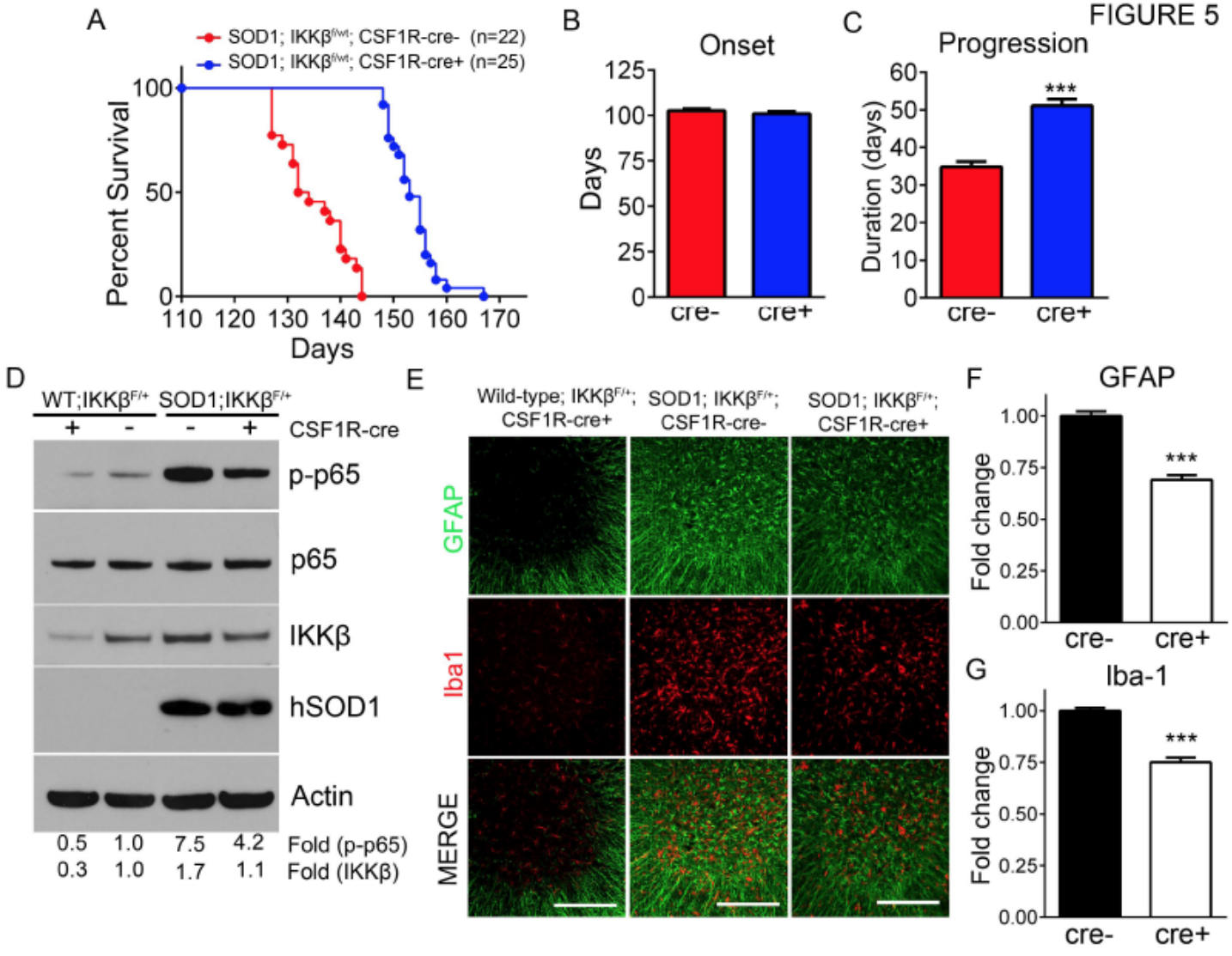
A
SOD1; IKKβ^fl/wt; CSF1R-cre- (n=22)
SOD1; IKKβ^fl/wt; CSF1R-cre+ (n=25)
Percent Survival
Days
B
Onset
Days
cre-
cre+
C
Progression
Duration (days)
***
D
WT;IKKβ^F/+
SOD1;IKKβ^F/+
CSF1R-cre
p-p65
p65
IKKβ
hSOD1
Actin
0.5 1.0 7.5 4.2 Fold (p-p65)
0.3 1.0 1.7 1.1 Fold (IKKβ)
E
Wild-type; IKKβ^F/+; CSF1R-cre+
SOD1; IKKβ^F/+; CSF1R-cre-
SOD1; IKKβ^F/+; CSF1R-cre+
GFAP
Iba1
MERGE
F
GFAP
Fold change
***
G
Iba-1
Fold change
***

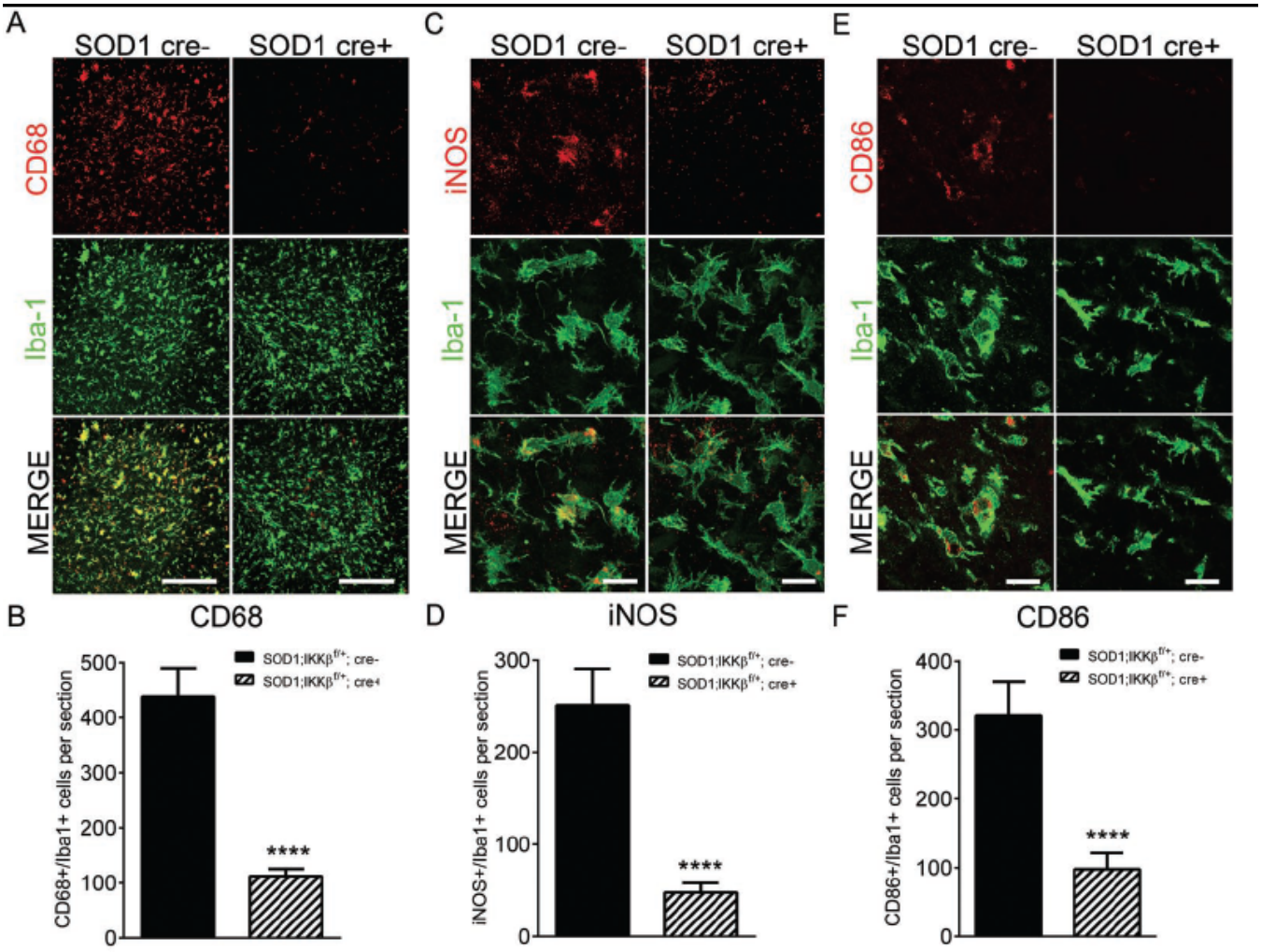
A
SOD1 cre-
SOD1 cre+
CD68
Iba-1
MERGE
C
SOD1 cre-
SOD1 cre+
iNOS
Iba-1
MERGE
E
SOD1 cre-
SOD1 cre+
CD86
Iba-1
MERGE
B
CD68
CD68+/Iba1+ cells per section
SOD1;IKKβf/+; cre-
SOD1;IKKβf/+; cre+
****
D
iNOS
iNOS+/Iba1+ cells per section
SOD1;IKKβf/+; cre-
SOD1;IKKβf/+; cre+
****
F
CD86
CD86+/Iba1+ cells per section
SOD1;IKKβf/+; cre-
SOD1;IKKβf/+; cre+
****

Figure 6

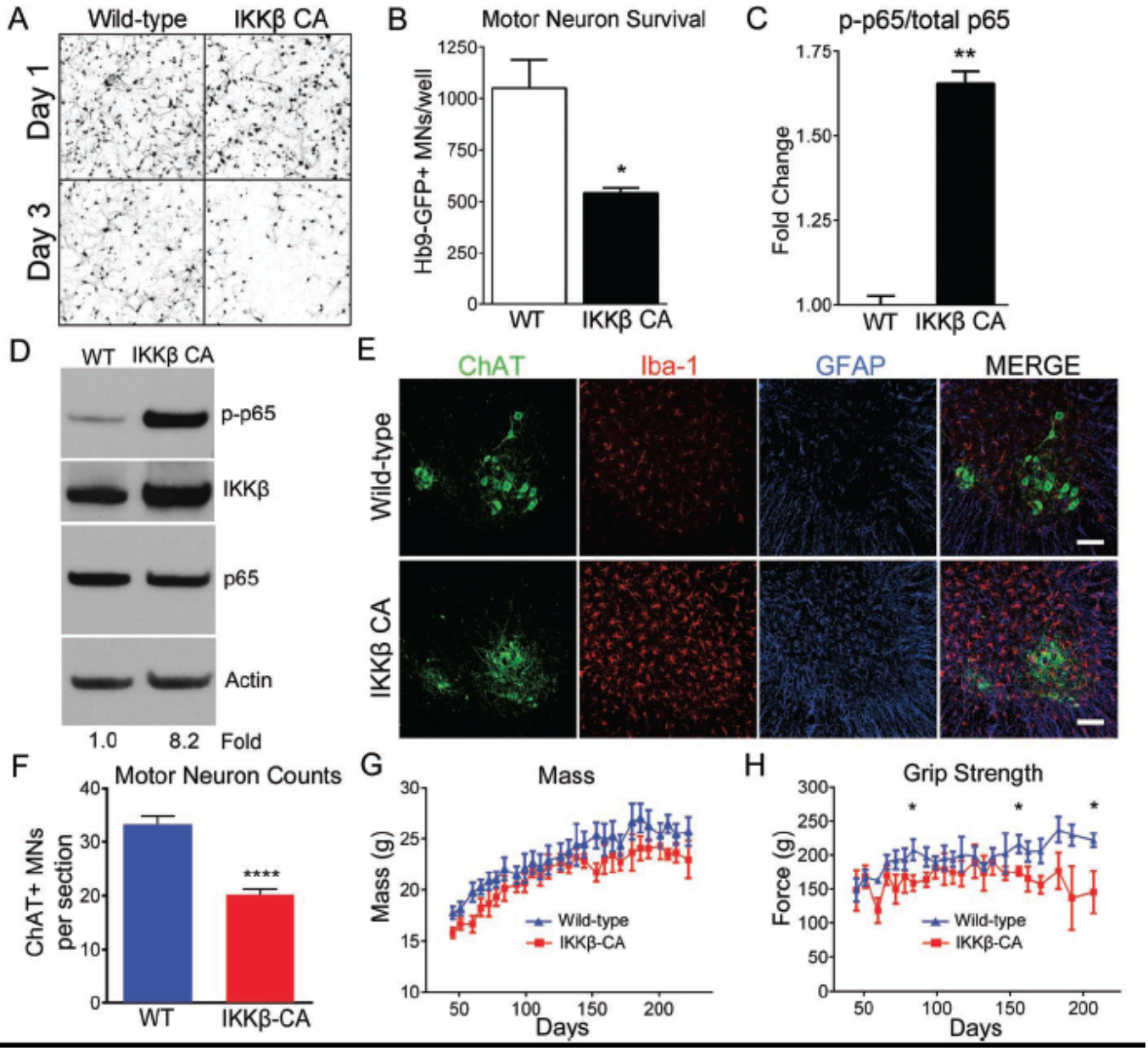
A
Wild-type
IKKβ CA
Day 1
Day 3
B
Motor Neuron Survival
Hb9-GFP+ MNs/well
1250
1000
750
500
250
0
*
WT
IKKβ CA
C
p-p65/total p65
Fold Change
1.75
1.50
1.25
1.00
**
WT
IKKβ CA
D
WT
IKKβ CA
p-p65
IKKβ
p65
Actin
1.0
8.2
Fold
E
ChAT
Iba-1
GFAP
MERGE
Wild-type
IKKβ CA
F
Motor Neuron Counts
ChAT+ MNs per section
40
30
20
10
0
****
WT
IKKβ-CA
G
Mass
Mass (g)
30
25
20
15
10
Wild-type
IKKβ-CA
50
100
150
200
Days
H
Grip Strength
Force (g)
300
250
200
150
100
50
0
*
*
*
Wild-type
IKKβ-CA
50
100
150
200
Days

Figure 7

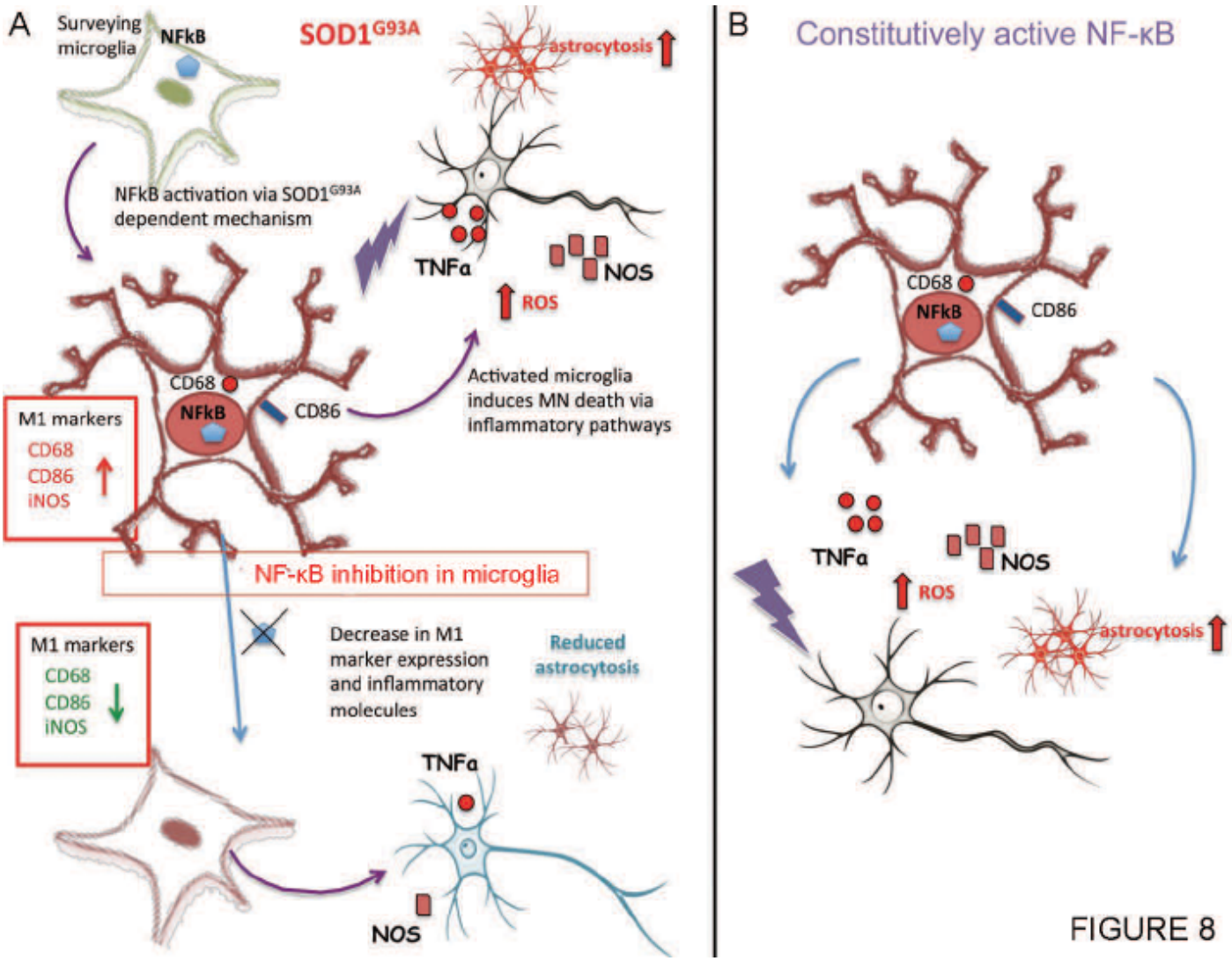
A
Surveying microglia
NFkB
SOD1G93A
astrocytosis
NFkB activation via SOD1G93A dependent mechanism
TNFα
NOS
ROS
CD68
NFkB
CD86
Activated microglia induces MN death via inflammatory pathways
M1 markers
CD68
CD86
iNOS
NF-κB inhibition in microglia
M1 markers
CD68
CD86
iNOS
Decrease in M1 marker expression and inflammatory molecules
Reduced astrocytosis
TNFα
NOS
B
Constitutively active NF-κB
CD68
NFkB
CD86
TNFα
NOS
ROS
astrocytosis

FIGURE 8

SUPPLEMENTAL FIGURES AND LEGENDS

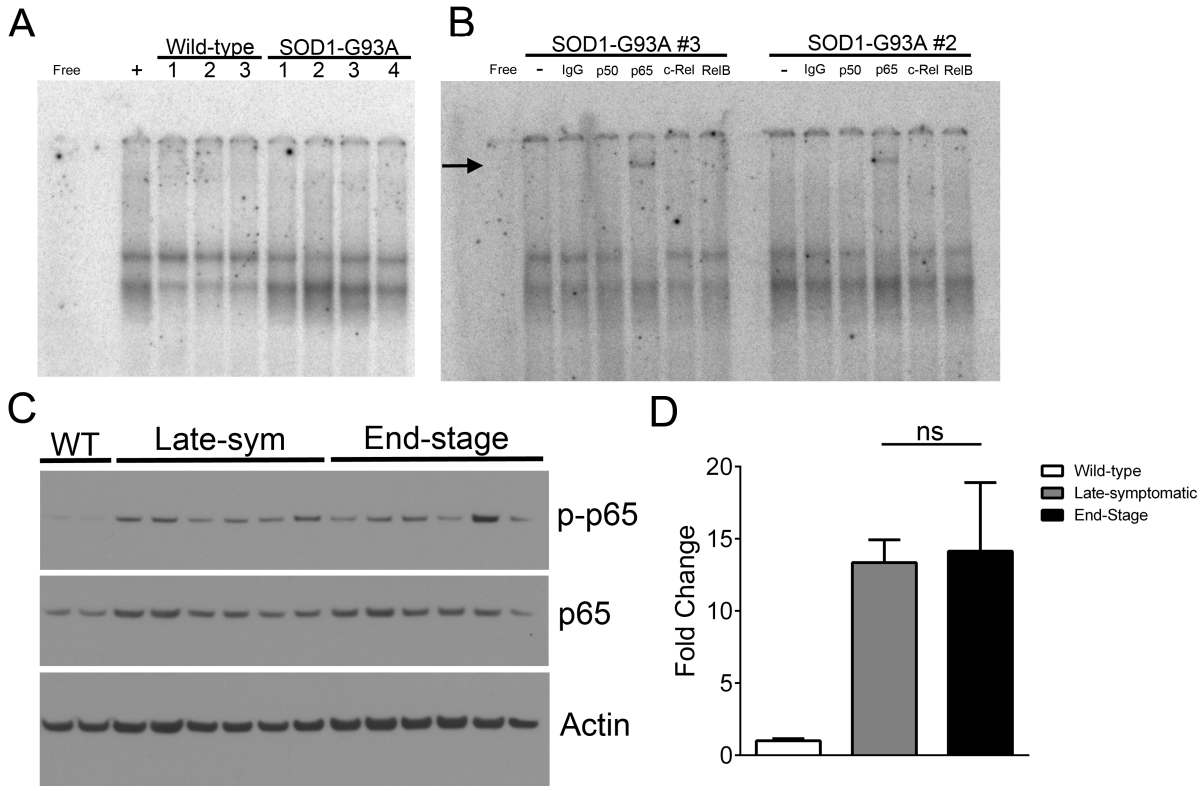

Figure S1. The classical NF-κB pathway is activated in SOD1-G93A mice, related to Figure 1.

(A) Electrophoretic mobility shift assay of total spinal cord nuclear extracts from 130 day old wild-type mice and end-stage SOD1-G93A mice. Free represents the probe free condition. "+" represents positive control from IKKβCA mice.

(B) Supershifts of nuclear extracts from SOD1-G93A sample #3 and #2. Arrow shows supershifted band from p65 antibody. "-" indicates no antibody is added.

(C) Immunoblot of lumbar spinal cord protein lysate from wild-type (n=2), late-stage (n=6), and end-stage (n=6) SOD1-G93A mice. The blot was probed for phospho-p65 and reprobed for total p65 (middle) and Actin (bottom) as loading controls.

(D) Fold change of the immunoblot in (C) determined using Image J to measure band intensities of phospho-p65 normalized to p65/Actin. Phospho-p65 is upregulated by 13.4 ± 1.6 fold compared to wild-type at the late-symptomatic stage and by 14.1 ± 4.8 fold at end stage. Error bars represent s.e.m.

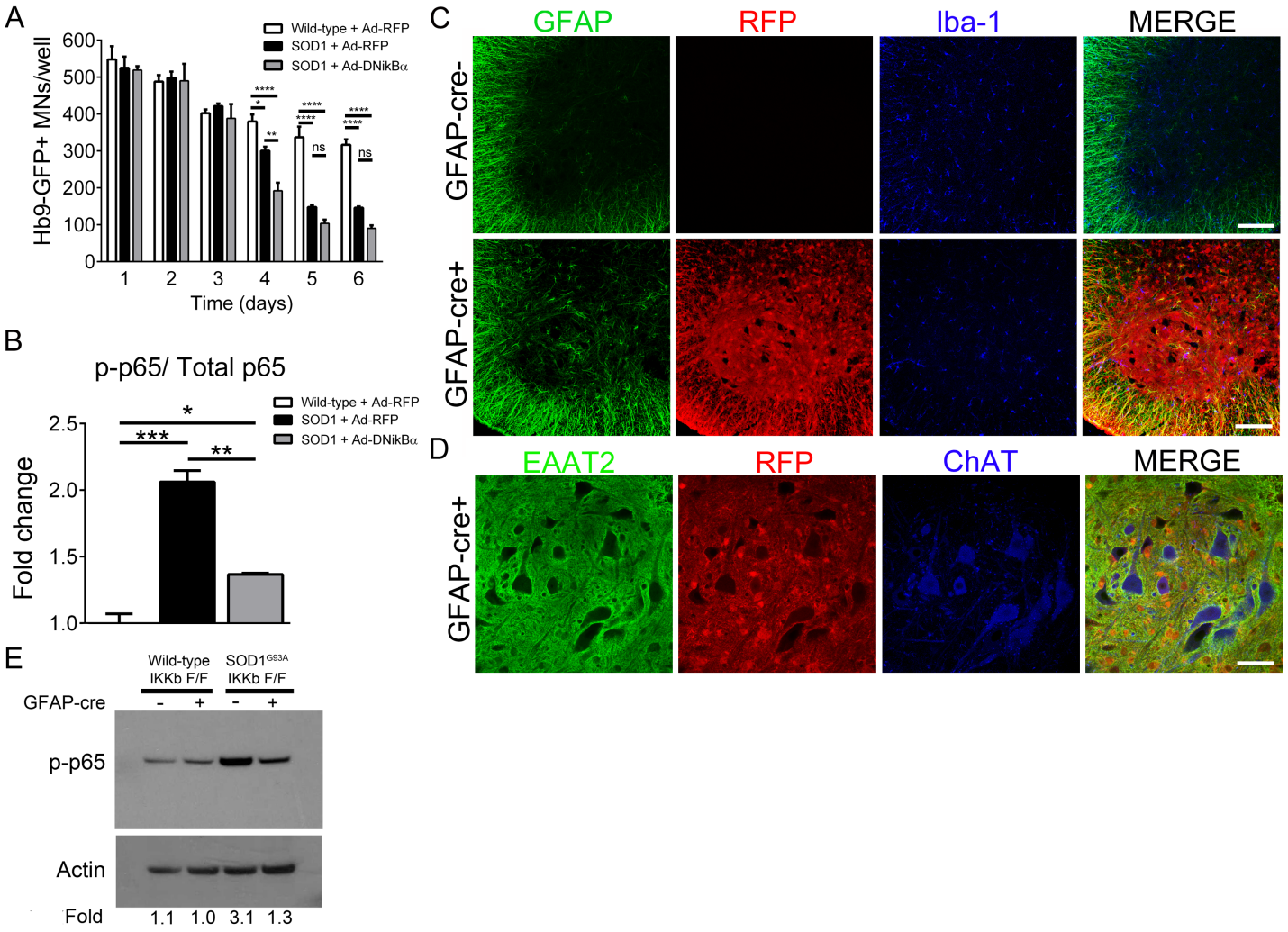

Figure S2. NF-κB inhibition in astrocytes does not confer neuroprotection *in vitro* or *in vivo* in the SOD1-G93A mouse model, related to Figure 1.

(A) Quantification of surviving Hb9-GFP+ motor neurons per well during 6-day co-culture with wild-type (white) or SOD1-G93A astrocytes infected with Ad-RFP (black) or Ad-IκBα-SR (gray). (n=3)

(B) Quantification of phospho-p65 by ELISA in wild-type and SOD1-G93A astrocytes infected by Ad-RFP or Ad-IκBα-SR and stimulated with 10ng/mL TNF-α for 12 hours.

(C and D) Representative images of GFAP-cre-negative and positive Rosa26-Stop^{Flox}-CAG-tdTomato mice. Native RFP fluorescence was analyzed for co-localization with immunohistochemical markers for (C) astrocytes (GFAP and EAAT2), microglia (Iba1), and (B) motor neurons (ChAT). Scale bar = 100 microns (top) 50 microns (bottom)

(E) Immunoblot of lumbar spinal cord protein isolated from WT; IKKβ$^{f/f}$; GFAP-cre-, WT; IKKβ$^{f/f}$; GFAP-cre+, and symptomatic SOD1-G93A; IKKβ$^{f/f}$; GFAP-cre-, SOD1-G93A; IKKβ$^{f/f}$; GFAP-cre+ mice probed for phospho-p65 (top) and Actin (bottom) confirm reduction in NF-κB activation in cre+ mice. Fold change represents band intensities of phospho-p65/Actin determined by ImageJ. Error bars represent s.e.m. * , P< 0.05; **, P<0.01; **** , P< 0.0001

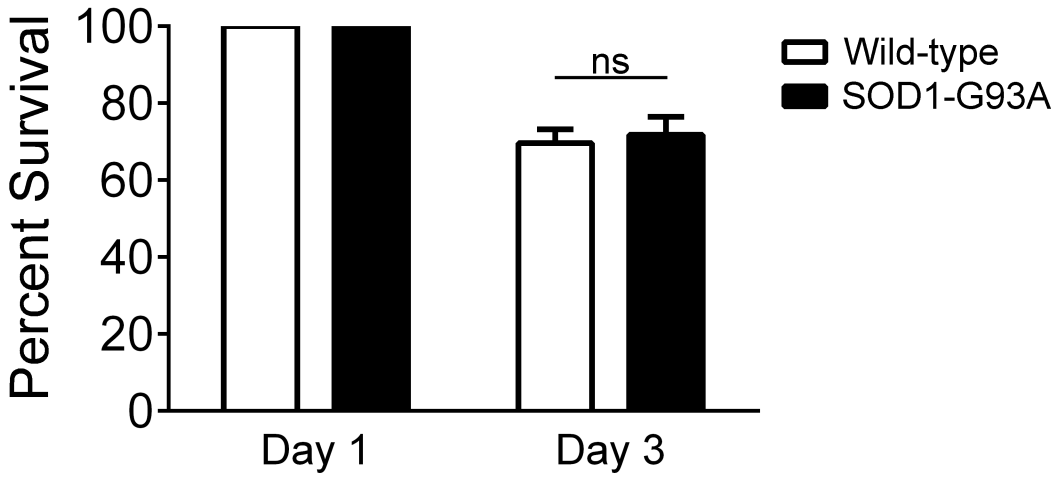

Figure S3. SOD1-G93A neonatal microglia are not toxic to Hb9-GFP+ motor neurons compared to wild-type microglia, related to Figure 4. Quantification of surviving Hb9-GFP+ motor neurons per well during co-culture with wild-type (white) or SOD1-G93A microglia (black). Error bars represent s.e.m.

Movie S1. Live-imaging of co-culture with Hb9-GFP+ motor neurons (green) and wild-type microglia (red), related to Figure 4.

Movie S2. Live-imaging of co-culture with Hb9-GFP+ motor neurons (green) and SOD1-G93A microglia (red), related to Figure 4.

Movie S3. Live-imaging of co-culture with Hb9-GFP+ motor neurons (green) and wild-type microglia overexpressing IκBα-SR (not fluorescently labeled), related to Figure 4.

Movie S4. Live-imaging of co-culture with Hb9-GFP+ motor neurons (green) and SOD1-G93A microglia overexpressing IκBα-SR (not fluorescently labeled), related to Figure 4.

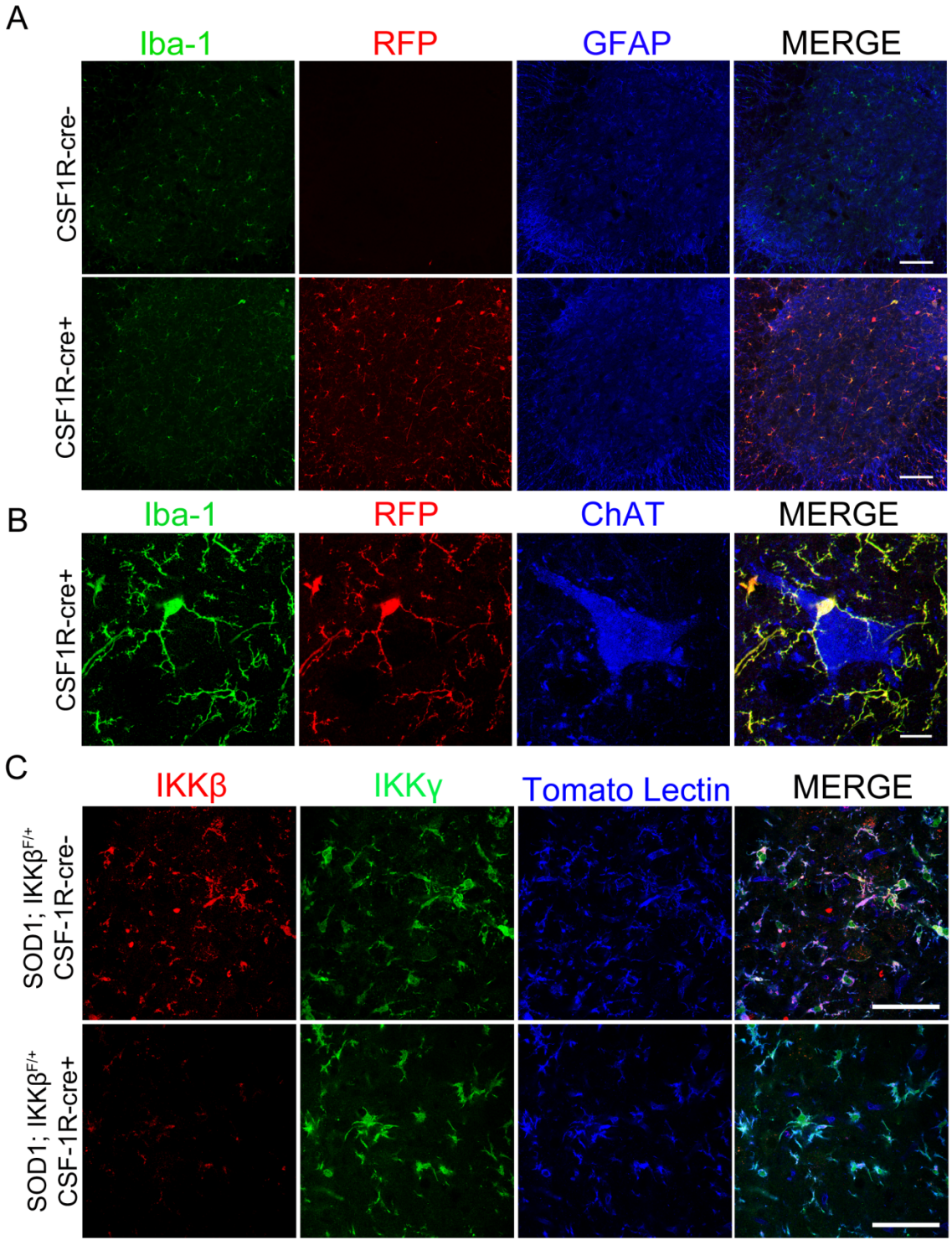

Figure S4. CSF-1R-cre is selectively expressed in microglia in the CNS, related to Figure 5. (A and B) Representative images of CSF1R-cre-negative and positive Rosa26-Stop^{Flox}-CAG-tdTomato mice. Native RFP fluorescence was analyzed for co-localization with immunohistochemical markers for (A) microglia (Iba-1) and astrocytes (GFAP), and (B) motor neurons (ChAT). Scale bar= 100 microns (top) and 10 microns (bottom).

(C) Immunohistochemical analysis of end-stage SOD1-G93A; IKKβ$^{F/wt}$; CSF1R-cre negative and positive mice for IKKβ (red) and IKKγ (green) and tomato lectin (blue). Scale bar = 50 microns

Movie S5. Movie of representative SOD1-G93A; IKKβ$^{f/wt}$; CSF-1R-cre+ mouse compared to cre-negative littermate. Related to Figure 5.

Movie S6. Live-imaging of co-culture with Hb9-GFP+ motor neurons (green) and wild-type microglia expressing constitutively active IKKβ (not fluorescently labeled). Related to Figure 7.

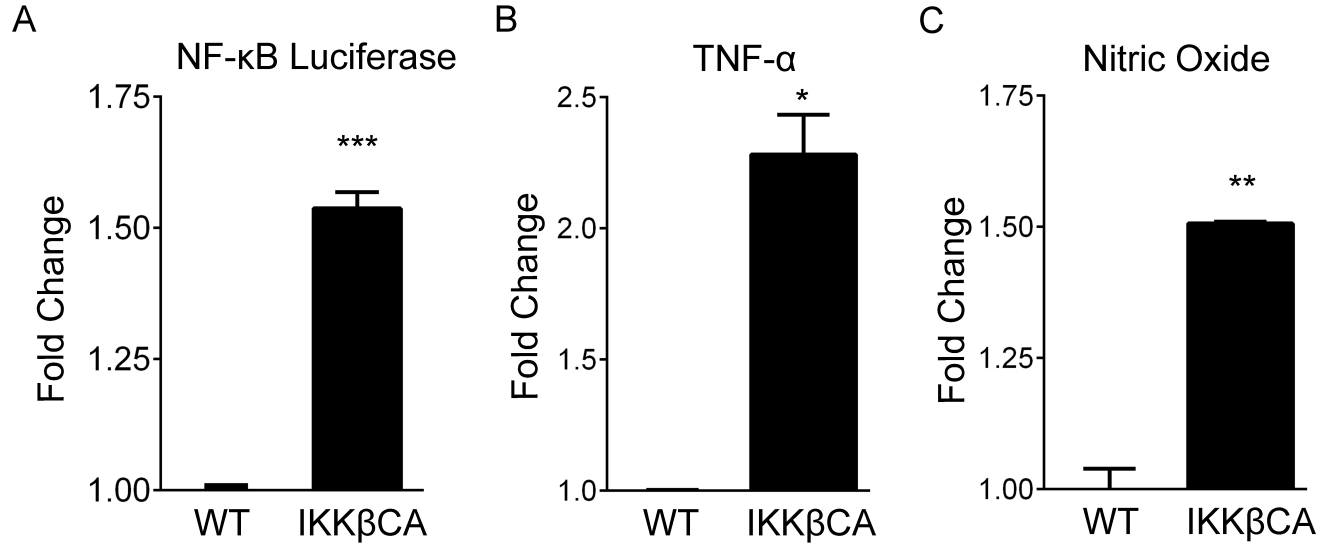

Figure S5. NF-κB activation in wild-type microglia *in vitro* induces microglial activation to a pro-inflammatory, neurotoxic phenotype, related to Figure 7.

(A) Luciferase assay of NF-κB activity in wild-type (white bar) and IKKβCA (black bar) microglia. Firefly luciferase was normalized to renilla luciferase.

(B and C) Quantification of TNF-α (B) and nitric oxide (C) in the co-culture medium by ELISA. Nitric oxide measured indirectly by sum of nitrate and nitrite.

Error bars represent s.e.m. * , P< 0.05, ** , P< 0.01

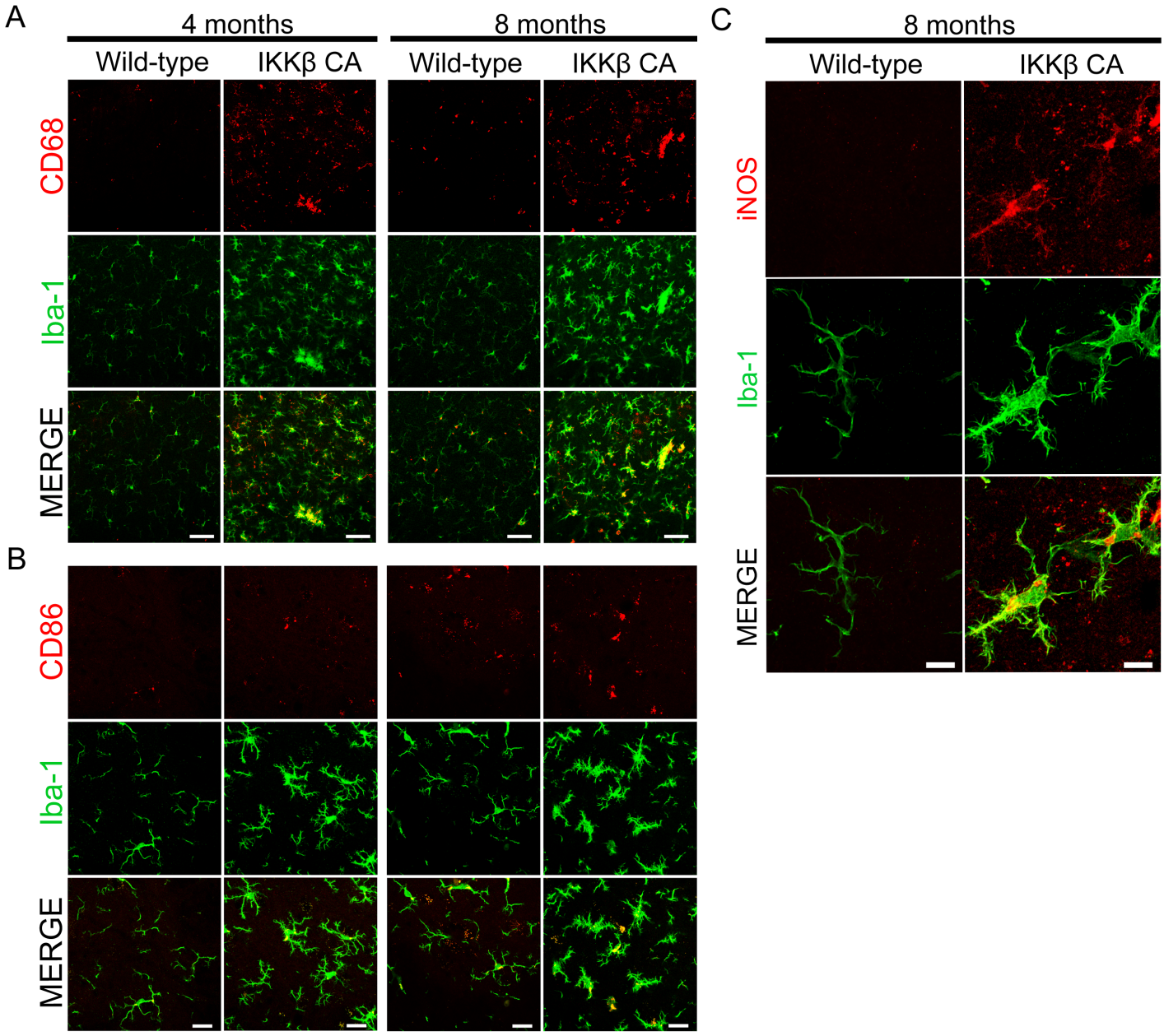

Figure S6. NF-κB activation in wild-type microglia *in vivo* induces microglial activation to a pro-inflammatory, neurotoxic phenotype, related to Figure 7.

(A) Immunohistochemistry of CD68 (red) and Iba1 (green) cells in lumbar spinal cord of WT and IKKβCA littermates at 4 and 8 months. Scale bar = 50 microns

(B) Immunohistochemistry of CD86 (red) and Iba1 (green) cells in lumbar spinal cord of WT and IKKβCA littermates at 4 and 8 months. Scale bar = 20 microns

(C) Immunohistochemistry of iNOS (red) and Iba1 (green) cells in lumbar spinal cord of WT and IKKβCA littermates at 8 months. Scale bar = 10 microns

SUPPLEMENTAL EXPERIMENTAL PROCEDURES

Supplemental Table 1. List of primers

Genotyping qualitative PCR

Gene	Forward Primer (5'-3')	Reverse Primer (5'-3')
human SOD1	CAT CAG CCC TAA TCC ATC TGA	CGC GAC TAA CAA TCA AAG TGA
Control for SOD1 reaction	CTA GGC CAC AGA ATT GAA AGA TCT	GTA GGT GGA AAT TCT AGC ATC ATC C
IKKβ	GTC ATT TCC ACA GCC CTG TGA	CCT TGT CCT ATA GAA GCA CAA
iCre	CAGGGCCTTCTCCACACCAGC	CTGGCTGTGAAGACCATC
Cre	GGACATGTTCAGGGATCGCCAGGCG	CGACGATGAAAGCATGTTTAGCTG
eGFP	GAG CTG AAG GGC ATC GAC TTC AAG	GGA CTG GGT GCT CAG GTA GTG G
negative for eGFP	TCAGGCCCACCTAGTCAGAT	AAAGCGGTCTGAGGAGGAA
tdTomato	CTG TTC CTG TAC GGC ATG G	GGC ATT AAA GCA GCG TAT CC
negative for tdTomato	AAG GGA GCT GCA GTG GAG TA	CCG AAA ATC TGT GGG AAG TC

Copy Number real time PCR

Primer	5' label	Sequence 5' --> 3'	3' Label
Transenic Probe	6-FAM	CTG CAT CTG GTT CTT GCA AAA CAC CA	Zen probe with Iowa Black
Internal Positive Control Forward	-	CAC GTG GGC TCC AGC ATT	-
Internal Positive Control Reverse	-	TCA CCA GTC ATT TCT GCC TTT G	-
hSOD1 Forward	-	GGG AAG CTG TTG TCC CAA G	-
hSOD1 Reverse	-	CAA GGG GAG GTA AAA GAG AGC	-
Internal Control Probe	Cy5	CCA ATG GTC GGG CAC TGC TCA A	Black Hole Quencher 2

Supplemental Table 2. List of antibodies

Western blot

Antibody	Dilution	Vendor
Phospho-p65	1:500	Cell Signaling
p65	1:500	Cell Signaling
Beta-Actin	1:1000	Cell Signaling
IKK-beta	1:125	Imgenex

Immunohistochemistry

Antibody	Dilution	Vendor
GFP	1:400	Abcam
Tomato Lectin	1:300	Vector Laboratories
GFAP	1:500	Abcam
Iba-1	1:400	Wako
CD68	1:100	AbDserotec
CD86	1:100	Millipore
iNOS	1:100	Sigma
IKK-gamma	1:100	Cell Signaling
IKK-beta	1:100	Imgenex

Immunocytochemistry

Antibody	Dilution	Vendor
CD11b	1:200	AbDserotec
F4/80	1:100	AbDserotec
NG2	1:200	Millipore
ChAT	1:100	Millipore
Iba-1	1:500	Wako
GFAP	1:200	Abcam

Flow Cytometry

Antibody	Dilution	Vendor
APC-CD11b	1:50	eBiosciences
PE-CD45	1:25	eBiosciences

EMSA supershift and nuclear western blots

p65	1:1000	Santa Cruz Biotechnology
p50	1:1000	Santa Cruz Biotechnology
c-Rel	1:1000	Santa Cruz Biotechnology
Rel-B	1:1000	Santa Cruz Biotechnology
IgG	1:1000	Santa Cruz Biotechnology

Transgenic mice

All procedures were performed in accordance with the NIH Guidelines on the care and use of vertebrate animals and approved by the Institutional Animal Care and Use Committee of the

Research Institute at Nationwide Children's Hospital. Animals were housed under light:dark (12:12 h) cycle and provided with food and water *ad libitum*. Transgenic female B6SJ/L(SOD1-G93A)1Gur/J mice and non-transgenic littermates (Jackson Laboratories) were utilized for time course immunoblot studies and primary cell isolations. Transgenic male B6SJ/L(SOD1-G93A)1Gur/J mice were used for breeding with other transgenic lines. SOD1 transgene copy number was confirmed by real time PCR. SOD1-G93A-NFκB^{EGFP} reporter mice were generated by breeding SOD1-G93A mice to C57BL/6 NFκB^{EGFP} mice (Christian Jobin) (Magness et al., 2004). SOD1-G93A; hGFAP-cre; IKK$\beta^{flox/flox}$ were generated by breeding SOD1-G93A mice to FVB hGFAP-cre (Jackson Labs) mice that had been crossed to C57BL/6 IKK$\beta^{flox/flox}$ mice (Li et al., 2003). SOD1-G93A; CSF-1R-icre; IKK$\beta^{flox/wt}$ were generated by breeding SOD1-G93A mice to C57BL/6 CSF-1R-cre mice (Deng et al., 2010) that had been bred to IKK$\beta^{flox/flox}$ mice. CSF1R-cre; IKKβCA were generated my breeding CSF-1R cre mice to C57BL/6 Rosa26-Stop^{Flox}IKKβCA mice (Jackson Labs). Cre specificity was confirmed by crossing cre lines to C57BL/6 Rosa26-Stop^{Flox}-CAG-tdTomato (Jackson Labs) mice and assessed for tdTomato expression by immunohistochemistry. Genotypes were determined by qualitative PCR using the primers in Supplementary Table 1.

Disease scoring and behavior analysis

Mice were classified as "pre-symtomatic" when they displayed no clinical symptoms of disease and had not reached peak weight. "Onset" was determined at the stage mice reach peak body weight. The "symptomatic" stage was determined when mice had lost 10% of their body weight and displayed motor impairment tremors or impaired hindlimb splay reflex. The "late-symptomatic" stage was determined when mice experienced pronounced hindlimb paralysis, but could reach food and water using forelimbs. "End-stage" was determined when animals could no longer "right" themselves within 30 seconds after the animal was placed on its back.

Testing of motor function using a rotarod device (Columbus Instruments, Columbus, OH) began at 50 days of age. Each session consisted of three trials that were averaged on the elevated accelerating rotarod beginning at 5 r.p.m./minute measuring the time the mouse was able to remain on the rod. Grip strength measurements for hindlimb were tested weekly using a grip strength meter (Columbus Instruments). Each session consisted of three tests per animal and values were averaged.

Immunoblot analysis

Cells and tissues were homogenized in Tissue Protein Extraction Reagent (Pierce) with EDTA, Complete protease inhibitor (Roche) and Phospho-STOP (Roche). The samples were run on NuPAGE Novex 4-12% Bis-Tris polyacrilamide gels and transferred to a PVDF membrane (Life Technologies). Blots were blocked in 5% milk powder, 0.5% BSA in PBS-Tween for 1h, and then incubated for overnight at 4°C with primary antibody. Bound primary antibody was detected by horseradish peroxidase conjugated secondary antibody followed by chemiluminescence detection (ECL Western Blot Substrate, Pierce). Antibodies are listed in Supplementary Table 2.

Immunohistochemistry

Animals were deeply anesthetized with a lethal dose of Xylazene/Ketamine and perfused transcardially with saline, then 4% paraformaldehyde. Spinal cords were sectioned 40 μm thick using a vibrating blade microtome (Leica microsystems). Sections were incubated for 2h at room temperature in TBS+ 1% Triton-X + 10% donkey serum. Samples were incubated for 72h at 4°C with primary antibodies, followed by 2h incubation at RT with secondary antibodies. All images were captured on a Zeiss confocal microscope (Carl Zeiss Microscopy, Thornwood, NY, USA). Antibodies are listed in Supplementary Table 2. For quantification of MNs and microglia, lumbar spinal cords were sectioned 40 μm thick from the end of thoracic level 14 to sacral level 1. For MN counts lumbar spinal cord sections were selected every 5th section from the first identifiable L1 section through L6 and sections were selected every 8th section for microglial quantification.

Electrophoretic mobility shift assays (EMSA) and nuclear western blots

EMSA and supershift analyses were performed on whole spinal cord nuclear lysates as previously described (Dahlman and Guttridge, 2012). Nuclear westerns were performed using the same nuclear lysates as used for the EMSAs. The antibodies against p65, p60, c-Rel, and RelB are listed in Supplementary Table 1.

Isolation and culture of adult primary astrocytes

Adult astrocyte cultures from brains of SOD1-G93A and wild-type littermates were prepared and purified as previously described (Miranda et al., 2012; Ray and Gage, 2006) with minor modifications. Enzymatically dissociated cells were cultured for 2 to 3 weeks, and then shaken overnight when the cells reached confluency to eliminate contaminating microglia. Adhered confluent astrocytes were treated with cytosine arabinose (20 μM) for 48 hours to kill rapidly dividing cells and microglia. Astrocytes were cultured in DMEM GlutaMAX^{TM} DMEM + 10% FBS + N2 + antibiotic-antimycotic (all from Life Technologies).

Isolation and culture of adult primary microglia

Adult microglia were isolated from brains of SOD1-G93A and WT littermates as previously described (Moussaud and Draheim, 2010) with minor modifications. 4-month old SOD1-G93A and WT littermate mice were deeply anesthetized and perfused transcardially with ice-cold Ringers solution (Fisher Scientific). Brains that appeared to not be fully exsanguinated were discarded. Brains were fragmented with a scalpel and incubated with an enzymatic solution containing papain for 60 minutes at 37°C, 5% CO2. The papain solution was quenched with 20% FBS in HBSS and centrifuged for 4 minutes at 200g. The pellet was resuspended in 2ml of 0.5 mg/ml DNase I (Worthington Biochemical) in HBSS and incubated for 5min at room temperature. The brain tissue was gently disrupted with fire-polished Pasteur pipettes and then filtered through a 70 micron cell strainer (Fisher Scientific) and centrifuged at 200g for 4 minutes. The resulting pellet was then

resuspended in 20ml of 20% isotonic Percoll (GE healthcare) in HBSS. 20mL of pure HBSS was carefully laid on top the percoll layer and centrifugation was performed at 200g for 20 min with slow acceleration and no brake. The interphase layer containing myelin and cell debris was discarded, and the pellet containing the mixed glial cell population was washed once with HBSS and suspended in Dulbecco's modified Eagle's/F12 medium with GlutaMAX^{TM} (DMEM/F12) supplemented with 10% heat inactivated FBS, antibiotic-antimycotic (all from Life Technologies) and 5 ng/ml of carrier-free murine recombinant granulocyte and macrophage colony stimulating factor (GM-CSF) (R&D systems). The cell suspension from four mouse brains were plated on a 15cm2 plate (Corning) coated with poly-l-lysine (Sigma) and maintained in culture at 37°C in a 95% air/ 5% CO2. The medium was replaced every 3 days until the cells reached confluency (after approximately 2 weeks). After the glial layer becomes confluent, microglia form a non-adherant, floating cell layer that can be collected, replated, and cultured for an extended period of time. After collecting the floating layer, microglia were incubated for 3 days without GM-CSF before re-plating for co-culture with MNs. Collected microglia were characterized by immunocytochemistry and flow cytometry (antibodies listed in Supplementary Table 1). Direct isolation of microglia for western blot analysis was performed as previously described (Cardona et al., 2006; Henry et al., 2009).

Isolation and culture of primary neonatal microglia

Microglia cultures were prepared from 3-day old SOD1-G93A and wild-type littermate pups as previously described with some minor modifications (Xiao et al., 2007). After removing meninges, cortices were dissociated and digested with 0.1% trypsin at 37°C for 15 minutes. Dulbecco's modified Eagle's medium (DMEM) supplemented with 10% FBS (Life Technologies) and DNase I (Worthington Biochemical) was added to the tissue homogenate. After centrifugation at 1200 RPM for 4 minutes, the cellular pellet was resuspended in DMEM with 10% FBS and plated 75cm^2 flasks. Medium was replaced 24 hours after plating. After 1 week incubation, the flasks were shaken

overnight at 250 RPM at 37°C. After collection, the microglia were plated for co-culture with motor neurons at a density of 6,000 cells per 96-well as described in the "Microglia/MN co-culture" experimental procedures section.

MN differentiation

Mouse embryonic stem cells expressing GFP driven by the Hb9 promoter (HBG3 cells, kind gift from Tom Jessell) were cultured on primary mouse embryonic fibroblasts (Millipore) and differentiated to MNs with the addition of 2 μM retinoic acid (Sigma) and 2 μM purmorphamine (Calbiochem). After 5 days of differentiation, the embryoid bodies were dissociated and sorted for GFP on a FACSVantage/DiVa sorter (Becton Dickinson).

ELISAs

TNFα Quantikine ELISA kit (R&D Systems) was used according to manufacturer instructions to quantify the TNFα concentration in co-culture medium. Nitric oxide levels in the co-culture medium were determined using the Total Nitric Oxide and Nitrate/Nitrite Parameter Kit (R&D Systems) according to manufacturer instructions. Co-culture medium was collected, centrifuged for 2 minutes at 200g, and 50uL of medium was added to each well for analysis. Phospho-p65 and Total p65 ELISA kits were used according to manufacturer instructions to quantify NF-κB activation in cell lysates (Cell Signaling). All conditions were tested in triplicate.

Virus production

Transgenic SOD1 expression in microglia was knocked down by lentiviral transduction expressing short interfering RNA sequences previously described (Haidet-Phillips et al., 2011; Miller et al., 2006). Lentivirus SOD1-shRNA and scramble-shRNA were produced by transient transfection into HEK293 cells using calcium phosphate, followed by supernatant viral purification by ultracentrifugation. Adenoviral vectors (Ad-RFP, Ad-cre, and Ad-IκBα-SR) were purchase from

Vector Biolabs. Microglia were infected with an MOI of 25 overnight, then washed with HBSS and incubated 3 days before co-culture with motor neurons.

AAV9-IκBα-SR injections

Adult tail vein injections were performed on 60 day old SOD1-G93A mice as previously described (Foust et al., 2008; 2010) with a 100 µl viral solution containing a mixture of PBS and 4×10^{12} DNase-resistant particles of scAAV9-CB- IκBα-SR (Virapur).

Flow cytometry of microglia cultures

Flow cytometric analysis of microglial cell surface markers was performed by first blocking Fc receptors with anti-CD16/CD32 antibody (eBiosciences, CA). Next, cells were incubated with anti-CD11b APC, anti-CD45 FITC (eBiosciences). Expression of these surface receptors was determined by flow cytometry using a Becton-Dickinson LSR II Cytometer. Ten thousand events were collected and microglia incubated with isotype control were used as a negative control. Flow data were analyzed using FlowJo software (Tree Star, San Carlos, CA).

Luciferase reporter assays

Primary microglia were plated at a density of 2×10^4 cells and transduced with 10 multiplicity of infection (MOI) of the inducible NFκB-responsive firefly luciferase reporter and 1 MOI of the cignal™ lenti renilla control using SureENTRY transduction reagent according to manufacturer manual (SABioscience). Adenoviral vectors encoding IκBα-SR and cre recombinase (Vector Biolabs) we used at an MOI of 25 to inhibit NF-κB. The cells were washed with PBS 24 hours post-infection. Firefly and renilla luciferase activities were determined using the Dual-Glo Luciferase Assay System (Promega) 72 hours after transduction. The amount of firefly luciferase activity of the transduced cells was normalized to renilla luciferase activity.

Supplemental References

Cardona, A.E., Huang, D., Sasse, M.E., and Ransohoff, R.M. (2006). Isolation of murine microglial cells for RNA analysis or flow cytometry. Nat Protoc *1*, 1947–1951.

Dahlman, J.M., and Guttridge, D.C. (2012). Detection of NF-κB activity in skeletal muscle cells by electrophoretic mobility shift analysis. Methods Mol. Biol. *798*, 505–516.

Deng, L., Zhou, J.-F., Sellers, R.S., Li, J.-F., Nguyen, A.V., Wang, Y., Orlofsky, A., Liu, Q., Hume, D.A., Pollard, J.W., et al. (2010). A novel mouse model of inflammatory bowel disease links mammalian target of rapamycin-dependent hyperproliferation of colonic epithelium to inflammation-associated tumorigenesis. Am. J. Pathol. *176*, 952–967.

Foust, K.D., Nurre, E., Montgomery, C.L., Hernandez, A., Chan, C.M., and Kaspar, B.K. (2008). Intravascular AAV9 preferentially targets neonatal neurons and adult astrocytes. Nat Biotechnol *27*, 59–65.

Foust, K.D., Wang, X., McGovern, V.L., Braun, L., Bevan, A.K., Haidet, A.M., Le, T.T., Morales, P.R., Rich, M.M., Burghes, A.H.M., et al. (2010). Rescue of the spinal muscular atrophy phenotype in a mouse model by early postnatal delivery of SMN. Nat Biotechnol *28*, 271–274.

Haidet-Phillips, A.M., Hester, M.E., Miranda, C.J., Meyer, K., Braun, L., Frakes, A., Song, S., Likhite, S., Murtha, M.J., Foust, K.D., et al. (2011). Astrocytes from familial and sporadic ALS patients are toxic to motor neurons. Nat Biotechnol *29*, 824–828.

Henry, C.J., Huang, Y., Wynne, A.M., and Godbout, J.P. (2009). Peripheral lipopolysaccharide (LPS) challenge promotes microglial hyperactivity in aged mice that is associated with exaggerated induction of both pro-inflammatory IL-1β and anti-inflammatory IL-10 cytokines. Brain Behavior and Immunity *23*, 309–317.

Li, Z.-W., Omori, S.A., Labuda, T., Karin, M., and Rickert, R.C. (2003). IKK beta is required for peripheral B cell survival and proliferation. J. Immunol. *170*, 4630–4637.

Magness, S.T., Jijon, H., van Houten Fisher, N., Sharpless, N.E., Brenner, D.A., and Jobin, C. (2004). In vivo pattern of lipopolysaccharide and anti-CD3-induced NF-kappa B activation using a novel gene-targeted enhanced GFP reporter gene mouse. J. Immunol. *173*, 1561–1570.

Miller, T.M., Kim, S.H., Yamanaka, K., Hester, M., Umapathi, P., Arnson, H., Rizo, L., Mendell, J.R., Gage, F.H., Cleveland, D.W., et al. (2006). Gene transfer demonstrates that muscle is not a primary target for non-cell-autonomous toxicity in familial amyotrophic lateral sclerosis. Proc. Natl. Acad. Sci. U.S.a. *103*, 19546–19551.

Miranda, C.J., Braun, L., Jiang, Y., Hester, M.E., Zhang, L., Riolo, M., Wang, H., Rao, M., Altura, R.A., and Kaspar, B.K. (2012). Aging brain microenvironment decreases hippocampal neurogenesis through Wnt-mediated survivin signaling. Aging Cell *11*, 542–552.

Moussaud, S., and Draheim, H.J. (2010). A new method to isolate microglia from adult mice and culture them for an extended period of time. Journal of Neuroscience Methods *187*, 243–253.

Ray, J., and Gage, F.H. (2006). Differential properties of adult rat and mouse brain-derived neural stem/progenitor cells. Mol. Cell. Neurosci. *31*, 560–573.

Xiao, Q., Zhao, W., Beers, D.R., Yen, A.A., Xie, W., Henkel, J.S., and Appel, S.H. (2007). Mutant SOD1 G93Amicroglia are more neurotoxic relative to wild-type microglia. J Neurochem *102*, 2008–

2019.